AD-A049 028 AEROSPACE CORP EL SEGUNDO CALIF IVAN A GETTING LABS F/G 20/5
O2(1 DELTA)-I ATOM ENERGY TRANSFER STUDIES: CW INVERSION ON 1.3--ETC(U)
DEC 77 R F HEIDNER, J G COFFER, C E GARDNER F04701-77-C-0078
UNCLASSIFIED TR-0078(3610)-1 SAMSO-TR-77-215 NL

OF
AD
A049028

END
DATE
FILMED
2-78
DDC

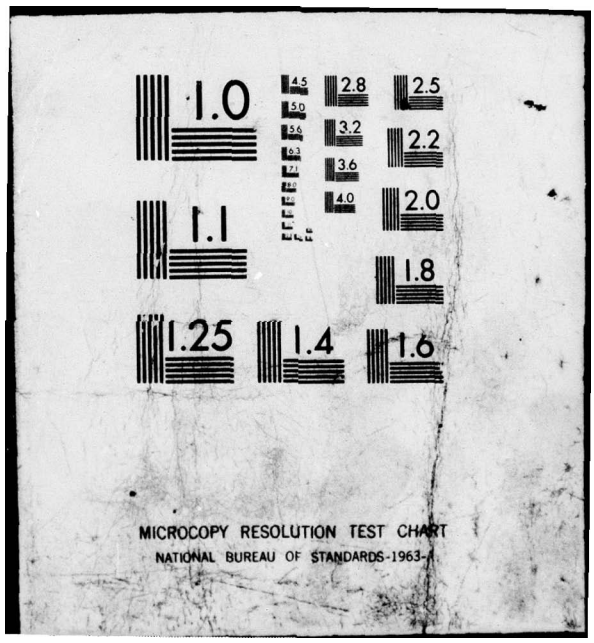
1.0
1.1
1.25
1.4
1.6
1.8
2.0
2.2
2.5
2.8
3.2
3.6
4.0
4.5
5.0
5.6
6.3
MICROCOPY RESOLUTION TEST CHART
NATIONAL BUREAU OF STANDARDS-1963-A

REPORT SAMSO-TR-77-215

$O_2(^1\Delta)$-I Atom Energy-Transfer Studies: CW Inversion on 1.315-μm I-Atom Transition

R. F. HEIDNER III, J. G. COFFER, and C. E. GARDNER
Aerophysics Laboratory
The Ivan A. Getting Laboratories
The Aerospace Corporation
El Segundo, Calif. 90245

15 December 1977

Interim Report

Prepared for
AIR FORCE WEAPONS LABORATORY
Kirtland Air Force Base, N. Mex. 87117

SPACE AND MISSILE SYSTEMS ORGANIZATION
AIR FORCE SYSTEMS COMMAND
Los Angeles Air Force Station
P.O. Box 92960, Worldway Postal Center
Los Angeles, Calif. 90009

This report was submitted by The Aerospace Corporation, El Segundo, CA 90245, under Contract F04701-77-C-0078 with the Space and Missile Systems Organization, Deputy for Advanced Space Programs, P. O. Box 92960, Worldway Postal Center, Los Angeles, CA 90009. It was reviewed and approved for The Aerospace Corporation by W. R. Warren, Jr., Director, Aerophysics Laboratory. Lieutenant Arturo G. Fernandez, SAMSO/YCPT, was the project officer for Advanced Space Systems.

This report has been reviewed by the Information Office (OI) and is releasable to the National Technical Information Service (NTIS). At NTIS, it will be available to the general public, including foreign nations.

This technical report has been reviewed and is approved for publication. Publication of this report does not constitute Air Force approval of the report's findings or conclusions. It is published only for the exchange and stimulation of ideas.

ARTURO G. FERNANDEZ, Lt, USAF
Project Officer

ROBERT W LINDEMUTH, Lt Col, USAF
Chief, Technology Plans Division

FOR THE COMMANDER

LEONARD E BALTZELL, Col, USAF
Asst. Deputy for Advanced Space Programs

UNCLASSIFIED

SECURITY CLASSIFICATION OF THIS PAGE (When Data Entered)

REPORT DOCUMENTATION PAGE

READ INSTRUCTIONS BEFORE COMPLETING FORM

1. REPORT NUMBER: SAMSO-TR-77-215	2. GOVT ACCESSION NO.
3. RECIPIENT'S CATALOG NUMBER	
4. TITLE (and Subtitle): $O_2(^1\Delta)$-I ATOM ENERGY TRANSFER STUDIES: CW INVERSION ON 1.315-μm I-ATOM TRANSITION	5. TYPE OF REPORT & PERIOD COVERED: Interim rept.
	6. PERFORMING ORG. REPORT NUMBER: TR-0078(3610)-1
7. AUTHOR(s): Raymond F. Heidner III, John G. Coffer and Carrol E. Gardner	8. CONTRACT OR GRANT NUMBER(s): F04701-77-C-0078
9. PERFORMING ORGANIZATION NAME AND ADDRESS: The Aerospace Corporation, El Segundo, Calif. 90245	10. PROGRAM ELEMENT, PROJECT, TASK AREA & WORK UNIT NUMBERS
11. CONTROLLING OFFICE NAME AND ADDRESS: Air Force Weapons Laboratory, Kirtland Air Force Base, N. Mex. 87117	12. REPORT DATE: 15 December 1977
	13. NUMBER OF PAGES: 85
14. MONITORING AGENCY NAME & ADDRESS (if different from Controlling Office): Space and Missile Systems Organization, Air Force Systems Command, Los Angeles, Calif. 90009	15. SECURITY CLASS. (of this report): Unclassified
	15a. DECLASSIFICATION/DOWNGRADING SCHEDULE

16. DISTRIBUTION STATEMENT (of this Report)

Approved for public release; distribution unlimited

17. DISTRIBUTION STATEMENT (of the abstract entered in Block 20, if different from Report)

DDC PROCURED JAN 23 1978 RESULTS F

18. SUPPLEMENTARY NOTES

19. KEY WORDS (Continue on reverse side if necessary and identify by block number)

CW Iodine Laser
Electronic Energy Transfer
Electronically Excited Oxygen
Flow-Tube Kinetic Studies
Ozone Photolysis

20. ABSTRACT (Continue on reverse side if necessary and identify by block number)

Low-temperature ozone photolysis (LTOP) has been developed as a cw source of $O_2(a^1\Delta_g)$. This method yielded large $O_2(^1\Delta)/O_2(^3\Sigma)$ ratios in a chemically "clean" system. Iodine was injected into a flowing stream of the LTOP products, and the fast energy-transfer process between $O_2(^1\Delta)$ and $I(^2P_{3/2})$ created a population inversion, $[I(^2P_{1/2})]/[I(^2P_{3/2})] \geq 0.5$, on the I-atom laser transition at 1.315 μm.

→ next page

DD FORM 1473 (FACSIMILE)

UNCLASSIFIED

SECURITY CLASSIFICATION OF THIS PAGE (When Data Entered)

409 944

19. KEY WORDS (Continued)

$a_1^{\ 1}\Delta_g$

20. ABSTRACT (Continued)

The development of quantitative diagnostic techniques for the O_2-I_2 system and their application to both electrical discharge and LTOP generation of $O_2(a^1\Delta_g)$ are described in this report. Emphasis is on the scaling required to produce a cw I-atom laser based on this latter experimental method.

PREFACE

We are pleased to thank S. N. Suchard and R. W. F. Gross for their continuing interest in and encouragement of this project. We would also like to acknowlege AFWL personnel Colonel Brabson, Major D. Olson, Dr. MacKnight Dr. Hadley, and their collaborators for their many suggestions. Several conversations with Professor G. Glass, Rice University, were of particular value.

Many thanks are due M. A. Kwok for the loan of equipment and help with testing the intrinsic Ge detector. The cw photolysis apparatus was designed by R. W. F. Gross. The O_3 generator was loaned by Professor C. Wittig, University of Southern California. K. L. Foster performed the NEST calculations and wrote the PDP-11 computer program for reducing the experimental data.

CONTENTS

FIGURES

FIGURES (Continued)

TABLES

I. INTRODUCTION

In 1964, J. V. V. Kasper, then a graduate student in G. C. Pimentel's laboratory, discovered the first photochemical laser.[1] This laser operated on the spin-orbit transition of the iodine atom at 1.315 μm. The photochemical I-atom laser has been extensively developed by researchers outside of the U.S.[2] and can presently deliver pulse energies of $\sim 10^3$ J and pulse powers $> 10^{12}$ W.[3] Since the I atom has a relatively small coefficient of stimulated emission (3×10^{-19} cm^2 at P_{Ar} = 1 atm)[3], large amounts of energy can be stored in a single laser device, making the I-atom laser attractive as a laser fusion device.[3]

For different applications, a cw I-atom laser would be attractive if it could be produced by chemical reaction or by an efficient energy-transfer scheme. The unsuccessful attempts to produce a population inversion in iodine with chemical reactions (e.g., O + HI) are not discussed in this report. Instead, the discussion concerns the most promising energy-transfer system presently known, i.e., the transfer of electronic energy from $O_2(^1\Delta)$ to $I(^2P_{3/2})$.

In 1966, Arnold, Finlayson, and Ogryzlo[4] observed that when I_2 was added to a gas stream containing $O_2(a^1\Delta_g)$ and $O_2(b^1\Sigma_g^+)$, a bright yellow flame appeared. This radiation was easily shown to be $I_2 B^3\Pi_{O_u^+} \rightarrow X^1\Sigma_g^+$ emission. In addition, a strong line appeared at 1.315 μm, which could only be the I-atom transition, $^2P_{1/2} \rightarrow {}^2P_{3/2}$. These authors postulated a mechanism for the dissociation of I_2, the behavior of $O_2(^1\Sigma)$, and the excitation of I^*, which later work has verified. First, the I_2 must be dissociated:†

$$I_2(^1\Sigma) + O_2(^1\Sigma) \underset{}{\overset{k_{15}}{\rightleftharpoons}} O_2(^3\Sigma) + 2I + \Delta E \qquad (\Delta E = 680 \text{ cm}^{-1}) \qquad (1)$$

†The numbering of rate coefficients corresponds to the complete model in Appendix A.

Second, I atoms must be excited to I^*:

$$I + O_2(^1\Delta) \underset{k_5}{\overset{k_1}{\rightleftharpoons}} O_2(^3\Sigma) + I^* + \Delta E \qquad (\Delta E = 279\ cm^{-1}) \qquad (2)$$

Third, the $O_2(^1\Sigma)$ must increase rather than decrease, as one would expect from Process (1). This increase in $O_2(^1\Sigma)$ occurs through Process (3):

$$O_2(^1\Delta) + I^* \xrightarrow{k_2} O_2(^1\Sigma) + I + \Delta E \qquad (\Delta E = 2364\ cm^{-1}) \qquad (3)$$

Fourth, the yellow emission must be explained. Arnold et al.[4] favored the three-body recombination of I and I^*;

$$I^* + I + M \rightarrow I_2(B^3\Pi_{O_u^+}) + M \qquad (4)$$

Derwent, Kearns, and Thrush[5] studied this system in much more detail, however, and established a more complicated mechanism for producing $I_2(B)$ (Figure 1):

$$O_2(^1\Sigma) + I_2(^1\Sigma) \xrightarrow{k_{16}} O_2(^3\Sigma) + I_2(^3\Pi_{1u}) + \Delta E \qquad (\Delta E = 1318\ cm^{-1}) \quad (5)$$

$$\xrightarrow{k_{15}} 2I + O_2(^3\Sigma) \qquad (1)$$

$$I_2(^3\Pi_{1u}) + O_2(^1\Delta) \rightarrow I_2(^3\Pi_{O_u^+}) + O_2(^3\Sigma) + \Delta E \qquad (\Delta E = 3960\ cm^{-1}) \quad (6)$$

In a series of papers, Derwent and Thrush[6-9] evaluated the rate coefficients for most of the critical chemical processes in this system (Appendix A).

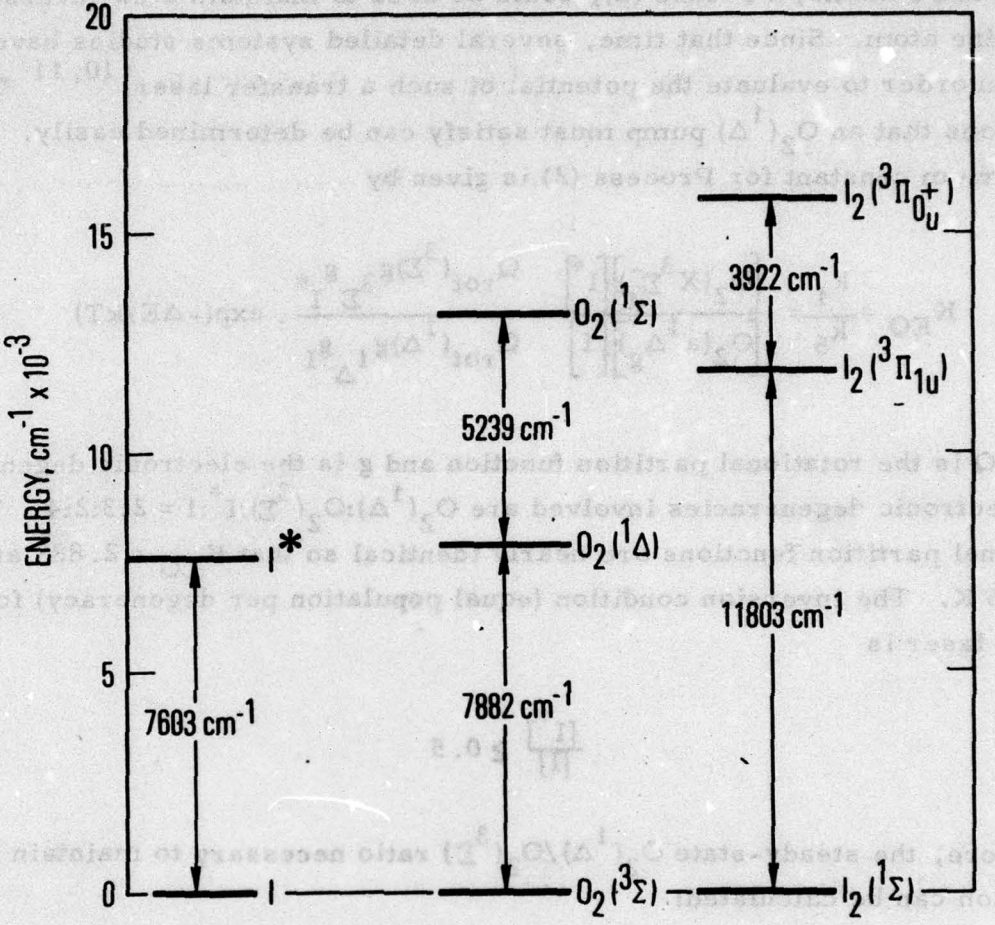

Figure 1. Electronic Energy Levels in O_2-I_2 System

They also made the first formal proposal[7] that energy transfer between $O_2(^1\Delta)$ and I atoms, Process (2), could be used to maintain a cw inversion in the iodine atom. Since that time, several detailed systems studies have been made in order to evaluate the potential of such a transfer laser.[10,11] The conditions that an $O_2(^1\Delta)$ pump must satisfy can be determined easily. The equilibrium constant for Process (2) is given by

$$K_{EQ} = \frac{k_1}{k_5} = \frac{\left[O_2(X^3\Sigma_g^-)\right]\left[I^*\right]}{\left[O_2(a^1\Delta_g)\right]\left[I\right]} = \frac{Q_{rot}(^3\Sigma)g_{3_\Sigma}\, g_{I^*}}{Q_{rot}(^1\Delta)g_{1_\Delta}\, g_I} \cdot \exp(-\Delta E/kT) \qquad (7)$$

where Q is the rotational partition function and g is the electronic degeneracy. The electronic degeneracies involved are $O_2(^1\Delta):O_2(^3\Sigma):I^*:I = 2:3:2:4$. The rotational partition functions are nearly identical so that $K_{EQ} = 2.88^\dagger$ at T = 295 K. The inversion condition (equal population per degeneracy) for the I-atom laser is

$$\frac{[I^*]}{[I]} \geq 0.5 \qquad (8)$$

Therefore, the steady-state $O_2(^1\Delta)/O_2(^3\Sigma)$ ratio necessary to maintain this inversion can be calculated:

$$\frac{[O_2(^1\Delta)]}{[O_2(^3\Sigma)]} = \left(\frac{[I^*]}{[I]}\right) \cdot K_{EQ}^{-1} = 0.174 \qquad (9)$$

The conditions necessary to produce a cw energy transfer iodine laser based on $O_2(^1\Delta)$ can be summarized as follows:

1. An $O_2(^1\Delta)/O_2(^3\Sigma)$ ratio greater than 0.174 must be obtained.

---

†Derwent and Thrush uniformly quote the value 2.94, although in one paper it is for T = 295 K and in another T = 298 K.

2. The equilibrium given by Process (2) must be rapidly attained, and side reactions must be relatively unimportant.

3. The $[O_2(^1\Sigma)]$ must be sufficient to dissociate the I_2 that is injected as an I-atom source.

4. A sufficient inversion density on the iodine atom transition must be obtained to overcome cavity losses.

Although most of the data in this report were obtained during FY 76, under contract to AFWL, preliminary studies performed under DARPA sponsorship are included to provide a more complete picture of this transfer system.

II. SUMMARY

The kinetic model described in the Introduction, and more completely in Appendix A, strongly indicates that a cw I-atom laser, based on energy transfer from $O_2(^1\Delta)$, can be constructed. Since the kinetic studies cited earlier[5-9] did not employ large $O_2(^1\Delta)/O_2(^3\Sigma)$ ratios, no one had demonstrated that I^*/I ratios > 0.5 could be observed in the laboratory. The present study has shown that, within limits, the relationship given in Eq. (9) is obeyed and that I^*/I ratios > 0.5 can be achieved in a continuous flow system. Thus, there appears to be no fundamental barrier to the construction of a cw I-atom laser.

The following, obtained under the present contract with AFWL, are significant factors in the attempt to scale the inversion density in the iodine system:

1. Characterization of the absolute densities of $O_2(^1\Delta)$ and $O_2(^1\Sigma)$ produced by a single 100-W microwave discharge in O_2.
2. The development of low-temperature ozone photolysis (LTOP) as a method of producing large $O_2(^1\Delta)/O_2(^3\Sigma)$ ratios.
3. The determination of the absolute densities of I^* and I in the O_2-I_2 system.
4. The effect of wall coatings on the deactivation of electronically excited O_2 and on I-atom recombination.
5. The role of $O_2(^1\Sigma)$ and possibly $O(^3P)$ in the dissociation of I_2 and identification of scaling problems.

The highest I^*/I ratio measured in the LTOP + I_2 experiments was 0.79 with an inversion density ($[I^*] - 1/2\,[I]$) of $3.8 \times 10^{11}/cm^3$. The inversion density required for 10% gain/m is $\sim 1.65 \times 10^{13}/cm^3$.[12,13]

III. EXPERIMENTAL

A. FLOW SYSTEM

The flow system was constructed almost entirely of quartz and pyrex with greaseless glass stopcocks used for valving. Vacuum connections were made with either O-ring seals (pyrex pipe) or deKhotinsky cement (ground-glass joints). Even in high-pressure gas lines, material such as tygon and polyflo tubing was avoided in favor of stainless steel and glass. A large liquid N_2-cooled glass trap separated the flow system from the core pumping system (a 900-cfm Stokes pump and Roots blower combination). The flow system has an untrapped static leak rate of ~2 mTorr/hr.

In general, an attempt was made to use extremely high purity gases. Most of the quenching rates in the O_2-I_2 system are small; however, the flow velocities used were also very small ($\leq$400 cm/sec). The $[O_2(^1\Sigma)]$ is demonstrably senstive to gas purity under these experimental conditions. For N_2 (Matheson, 99.995%) and O_2 (Matheson, 99.99%), high purity two-stage regulators were used. The gases were further purified by passing them at 1 atm through molecular sieves traps (Linde 5A), which were periodically baked-out under vacuum at elevated temperatures. Originally, these traps were cooled to -195 K; however, this procedure was found to have little effect on gas purity. SF_6 (Matheson, 99.99%) was used without further purification, although its addition decreased the $[O_2(^1\Sigma)]$ to a greater extent than the published rate coefficients had indicated.[14] Helium (Air Products, 99.99%) was further purified by passing the gas at 1 atm through molecular sieves, which had been baked-out under vacuum and then cooled to 77 K. Molecular I_2 was distilled in vacuo into a glass-bead packed vessel. This vessel was then filled with He at 17 psia (880 Torr), forming a mixture with an I_2 mole fraction of 3.1×10^{-4} at T = 295 K.[15] HI (Matheson, Inc, 98%) was found to be highly contaminated with H_2. Samples were distilled into a 5-liter flask with a cold finger held at 77 K, subjected to several

freeze-pump-thaw cycles, and diluted with high purity Ar to a total pressure of ~900 Torr. Ozone was generated by passing purified O_2 at ~18 psia through a high-voltage ac discharge. Originally, a homemade generator was employed. Much higher production rates were later obtained by using a commercial O_3 generator (Ozone Research Corp., Model 03V9-0).† The $O_3 + O_2$ products of the ozonizer flowed at 1-atm pressure through a Si gel trap held at 195 to 200 K. At this temperature, O_3 is adsorbed preferentially on the gel well above its boiling point, thus avoiding the detonation problems often encountered during O_3 liquifaction.[16] After a substantial amount of O_3 was collected (several grams in later experiments), the trap was pumped for several minutes to remove O_2. Nonindicating Si gel must be used, since the O_3 itself is a deep purple color. If care is exercised, the O_3 removed from the Si gel is > 90% pure, the residual being O_2. The O_3 is carried into the system by flowing N_2 through the trap. The concentration of O_3 is measured in situ by attenuation of 2537 Å radiation. A 10-cm cell provides good sensitivity over the 0.01 to 1.0 Torr pressure range (ϵ_e^{2537} = 0.35 cm^{-1} $Torr^{-1}$).[17]

The molar flow rates of N_2, O_2, SF_6, H_2, and He were measured with rotating ball flowmeters (Matheson) held at constant pressure by low-pressure regulators (Matheson). These flowmeters were calibrated by pressure rise measurements in a standard volume. The molar flow rates of He + HI and He + I_2 mixtures in the atomic resonance fluorescence measurements were measured by timing the pressure drop in calibrated 5-liter storage bulbs.

During these experiments, the following species were directly observed: $O_2(^1\Delta)$, $O_2(^1\Sigma)$, $I(^2P_{1/2})$, $I(^2P_{3/2})$, $I_2(^3\Pi_{O_u^+})$, and O_3. The following species concentrations were calculated from their molar flow rates: O_2, N_2, SF_6, and I_2(+ He). Measuring the absolute concentration of the upper and lower levels of a laser transition is clearly less satisfactory than a gain measurement; therefore, the experimental methods and the assumptions made will be dealt with in some detail.

---

†Kindly made available by Dr. Curt Wittig, Department of Electrical Engineering, University of Southern California.

The apparatus has evolved during experimentation; however, two distinct sections can be identified. Section 1 includes the ozone photolysis reactor, a small-diameter section compatible with a 100-W Evenson-type microwave cavity, a HgO-coated section for recombining O atoms,[18] and a movable isothermal calorimeter probe[19,20] for measuring $O_2(^1\Delta)$. Figure 2 is a schematic of this section, and Figure 3 is a photograph. Section 2 includes a kinetic flow tube and the associated spectroscopic diagnostics used to measure the species. Figure 4 is a schematic of all the diagnostics.

B. ISOTHERMAL CALORIMETRY

1. THEORY

This technique was originally used by Elias, Ogryzlo, and Schiff for $O_2(^1\Delta)$.[19] It has been refined for other studies by Kaufman and coworkers.[20] Bott and Heidner[21] used the technique for recent measurements of H-atom quenching of vibrationally excited hydrogen halides.

Briefly, the method works as follows: a coil of 0.010-in. Ni wire forms one arm of a Kelvin bridge circuit. This coil of wire is inserted into the gas stream and heated by an external power supply to an elevated temperature. At a temperature T (~150°C), the coil resistance is such that the bridge is balanced (Figure 5). The circuit design for the self-balancing bridge was taken from the work of Ham et al.[20] Thus, with no active species in the gas stream, the power dissipation of the coil is

$$W_{coil}(1) = i^2_{coil}(1) \cdot R_{coil} = i^2_{coil}(1) \cdot R_s \qquad (10)$$

When an active species in the gas stream can impart energy to the coil, the external circuit supplies only a fraction of the power necessary to heat the coil to the temperature T. The external circuit now supplies

$$W_{coil}(2) = i^2_{coil}(2) \cdot R_{coil} = i^2_{coil}(2) \cdot R_s \qquad (11)$$

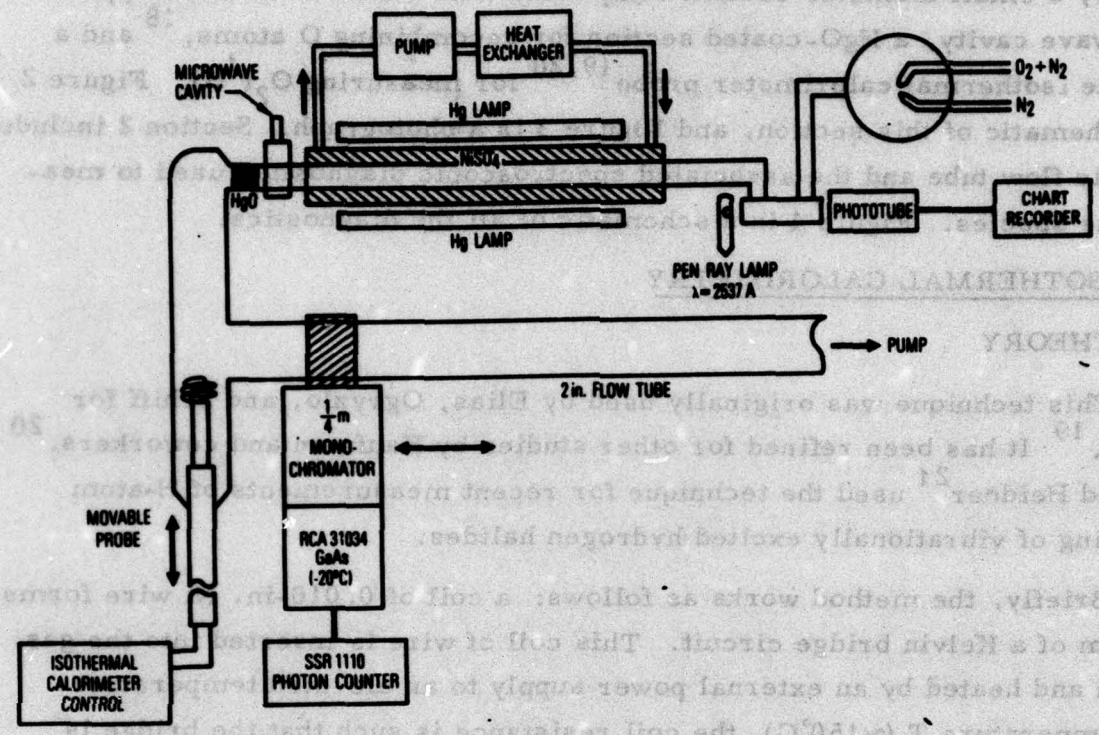

Figure 2. Continuous Photolysis Flow Tube

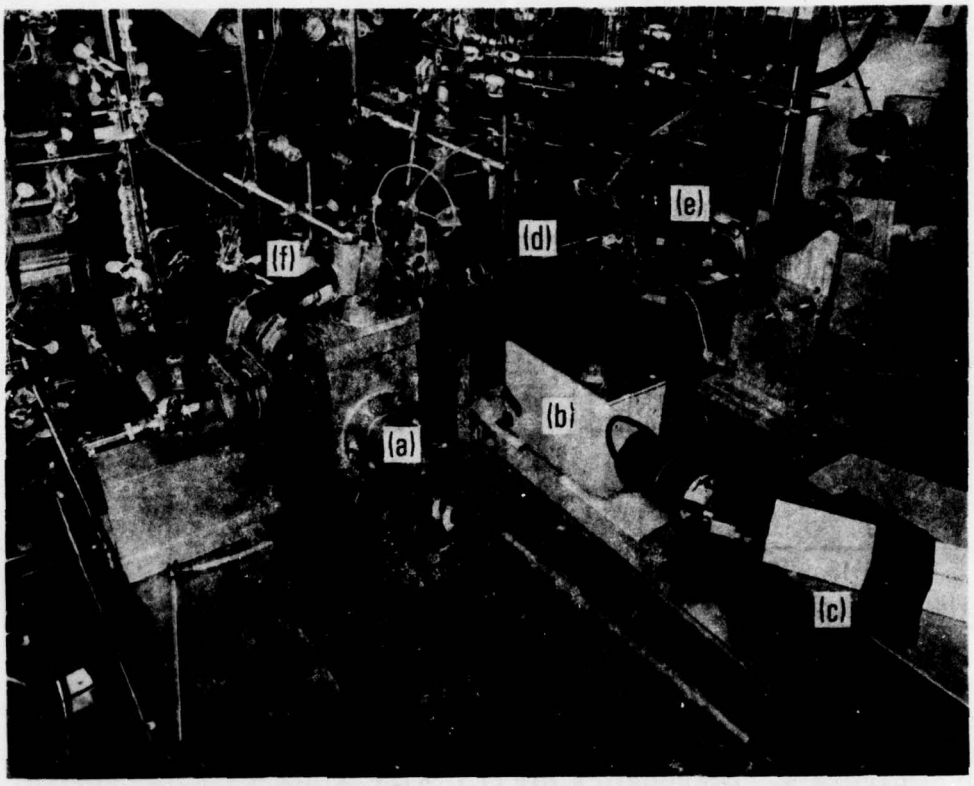

Figure 3. Low-Temperature Continuous-Photolysis Flow Tube and O_2^* Diagnostics. (a) Isothermal Calorimeter Probe. (b) Monochromator on Movable Platform. (c) Cooled GaAs Photomultiplier, Pulse Height Amplifier-Discriminator and Photon Counter. (d) Low-Temperature CW Photolysis Apparatus. (e) In Situ O_3 Diagnostic (2537-Å Lamp, 10-cm Absorption Cell, Photomultiplier). (f) Microwave Discharge Region and HgO Surface for O-Atom Recombination.

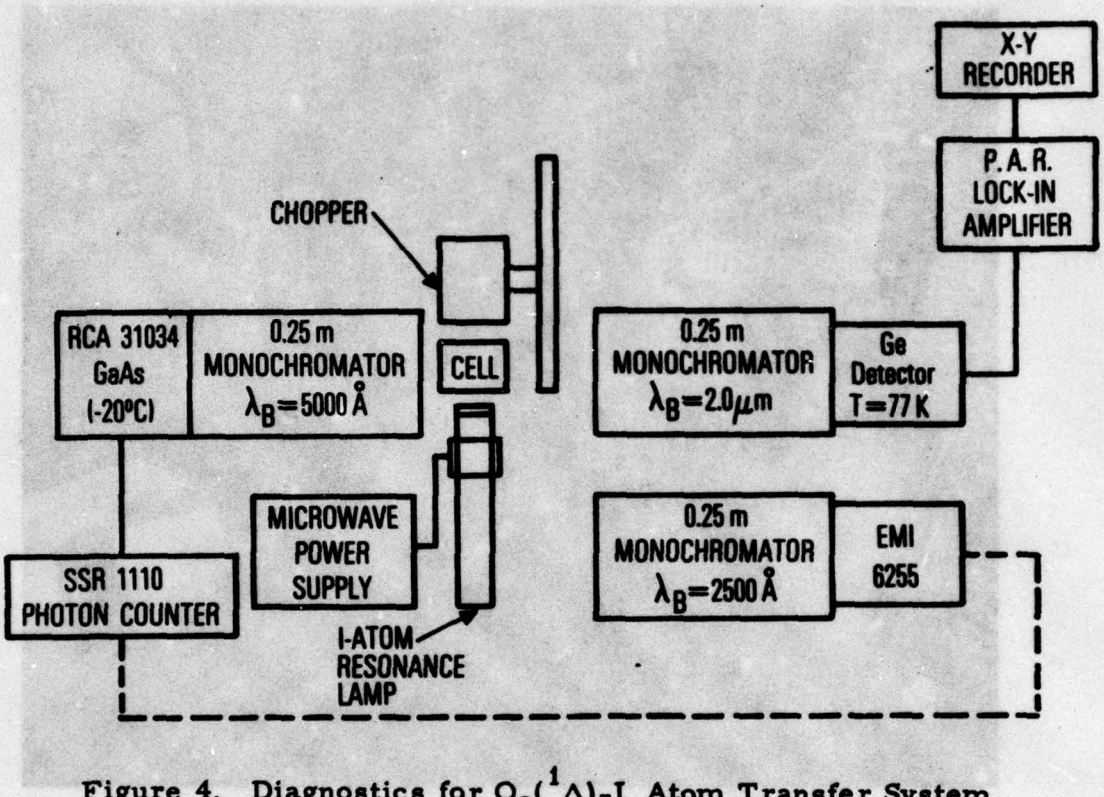

Figure 4. Diagnostics for $O_2(^1\Delta)$-I Atom Transfer System

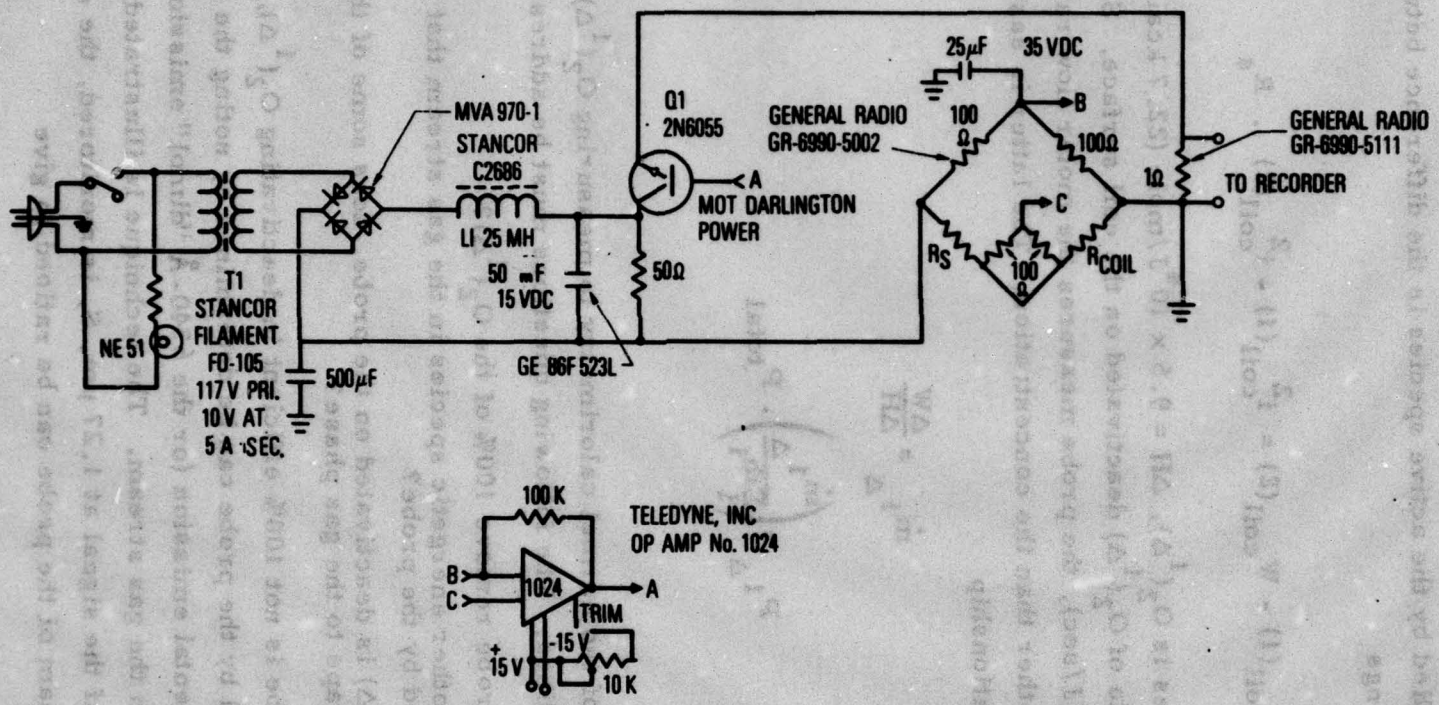

Figure 5. Self-Balancing Isothermal Calorimeter Circuit

Thus, the power supplied by the active species is the difference between these two power readings

$$\Delta W = W_{coil}(1) - W_{coil}(2) = i^2_{coil}(1) - i^2_{coil}(2) \cdot R_s \qquad (12)$$

When the active species is $O_2(^1\Delta)$, $\Delta H = 9.5 \times 10^4$ J/mole (22.7 kcal/mole) is imparted for each mole of $O_2(^1\Delta)$ deactivated on the coil surface. Since the coil measures power (J/sec), the probe measures the molar flow rate of $O_2(^1\Delta)$ (moles/sec) rather than the concentration. The latter is easily determined by the relationship

$$\dot{m}_{1_\Delta} = \frac{\Delta W}{\Delta H} \qquad (13)$$

$$P_{1_\Delta} = \left(\frac{\dot{m}_{1_\Delta}}{\sum_i \dot{m}_i}\right) \cdot P_{total} \qquad (14)$$

2. LIMITATIONS

The application of isothermal calorimetry to measuring $O_2(^1\Delta)$ is not quite as simple as outlined. The following questions must be addressed:

1. Does the probe remove 100% of the $O_2(^1\Delta)$?
2. Are there other energetic species in the gas stream that will be recorded by the probe?
3. When $O_2(^1\Delta)$ is deactivated on the probe, does some of the energy escape to the gas phase?

Although the probe is not 100% efficient in deactivating $O_2(^1\Delta)$, the fraction of $^1\Delta$ removed by the probe can be determined by noting the decrease in the 1.27-μm fundamental emission (or the 6340-Å "dimol" emission) when the probe is inserted in the gas stream. The technique is illustrated in Figure 6. For example, if the signal at 1.27 μm, S, is monitored, the signals downstream and upstream of the probe can be ratioed to give

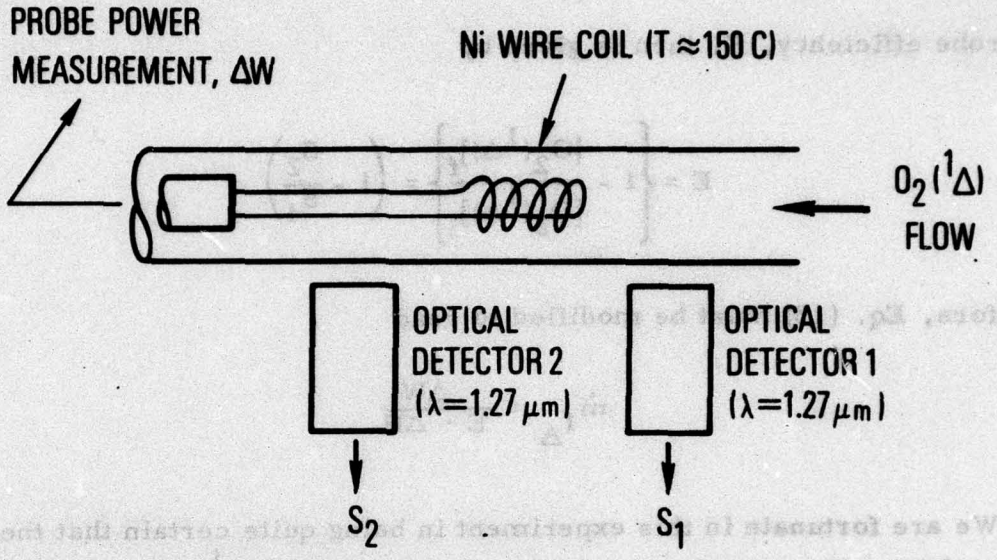

Figure 6. Isothermal Calorimetric Probe Efficiency Measurement

$$\frac{S_2}{S_1} = \frac{C[O_2(^1\Delta)]_f}{C[O_2(^1\Delta)]_i} \tag{15}$$

The probe efficiency, E, then is given by

$$E = \left\{1 - \frac{[O_2(^1\Delta)]_f}{[O_2(^1\Delta)]_i}\right\} = \left(1 - \frac{S_2}{S_1}\right) \tag{16}$$

Therefore, Eq. (13) must be modified to read

$$\dot{m}_{^1\Delta} = \frac{\Delta W}{E \cdot \Delta H} \tag{17}$$

We are fortunate in this experiment in being quite certain that the energy content of minority constituents such as O atoms and $O_2(^1\Sigma)$ is small compared with the energy content of $O_2(^1\Delta)$. Thus, the measured probe signal is due entirely to the deactivation of $O_2(^1\Delta)$. It is not known positively that all of the energy appears as probe signal when an $O_2(^1\Delta)$ molecule is deactivated. When H atoms recombine on a probe, it is known that the H_2 formed is not vibrationally excited.[20,22] Expressed in different language, all the recombination energy appears on the probe or the "accomodation coefficient" for the energy is unity. If the accomodation coefficient should turn out to be < 1, the $[O_2(^1\Delta)]$ in this study will have been underestimated, which is the preferable direction of error.

C. SPECTROSCOPY

The relevant spectroscopy of the O_2 and I_2 systems is summarized in Table I. Methods previously used to absolutely calibrate emission intensities include blackbody calibration, absolute radiance of the NO + O chemiluminescence,[23] ESR measurements on the excited state,[24] and measurement of

Table I. Spectroscopy of the O_2-I Atom Transfer System

Chemical Species	Electronic Transition	Observation Technique	Radiative Lifetime	Wavelength	Detector
$O_2(^1\Delta)$	$a^1\Delta_g \rightarrow X^3\Sigma_g^-$	Emission	3660 sec[27]	1.27 μm	Ge (T = 77 K)
$\{O_2(^1\Delta) - O_2(^1\Delta)\}$	$(a^1\Delta, a^1\Delta) \rightarrow (X^3\Sigma, X^3\Sigma)$	Emission	16 ± 4 cm^3/mol-sec[6]	6340 Å	GaAs (T = 253 K) RCA 31034
$O_2(^1\Sigma)$	$b^1\Sigma_g^+ \rightarrow X^3\Sigma_g^-$	Emission	13 sec[28]	7619 Å	GaAs (T = 253 K)
I_2	$B^3\Pi_{0_u^+} \rightarrow X^1\Sigma_g^+$	Emission	~5 × 10^{-7} sec[29]	5800 Å	GaAs (T = 253 K)
I^*	$^2P_{1/2} \rightarrow {}^2P_{3/2}$	Emission	0.128 sec[30]	1.315 μn	Ge (T = 77 K)
I^*	$^2P^{\uparrow}_{3/2} \leftrightarrow {}^2P_{1/2}$	Resonance Fluorescence	< 3.6 nsec[39]	2062 Å	S - 11 (T = 295 K) EMI 6256
I	$^4P^{\uparrow}_{5/2} \leftrightarrow {}^2P_{3/2}$	Resonance Fluorescence	90 ± 30 nsec[39]	1830 Å	S - 11 (T = 295 K) EMI 6256

the excited-state density with isothermal calorimetry.[19,25] The present work has utilized isothermal calorimetry to measure the $O_2(^1\Delta)$; both the 1.27-μm fundamental emission and the 6340-Å "dimol" emission have been calibrated against the calorimetric probe.

1. $O_2(^1\Delta)$ EMISSION FEATURES

Ogryzlo and coworkers[25,26] identified the broad emission band at 6340 Å as a cooperative emission of a single photon by two $O_2(^1\Delta)$ molecules

$$O_2(^1\Delta) + O_2(^1\Delta) \xrightarrow{k_r} O_2(^3\Sigma) + O_2(^3\Sigma) + h\nu \qquad (18)$$

Derwent and Thrush[6] measured the radiative collision rate coefficient, k_r, to be 16 ± 4 cm^3/mol-sec. The emission intensity should depend on $[O_2(^1\Delta)]^2$ whereas the fundamental emission at 1.27 μm obviously depends on $[O_2(^1\Delta)]$. Figure 7 is a plot of I_{6340} versus $(\dot{m}_{^1\Delta})^2$. The detection system for 6340 Å was highly stable over long periods of time, so that the absolute concentration of $O_2(^1\Delta)$ was determined on a day-to-day basis by this emission intensity. The Ge detector used to measure the $^1\Delta \rightarrow {}^3\Sigma$ emission at 1.27 μm and the $I^* \rightarrow I$ emission at 1.315 μm does not have good long-term stability. For this reason, $I_{1.27}$ was calibrated against I_{6340} for each run.

2. $O_2(^1\Sigma)$ EMISSION

The $^1\Sigma \rightarrow {}^3\Sigma$ emission at 7619 Å "dimol" emission. The concentrations of $O_2(^1\Delta)$ and $O_2(^1\Sigma)$ can be seen to be interrelated by the following equation:

$$\frac{[(O_2(^1\Sigma)]}{[O_2(^1\Delta)]^2} = \frac{k_r}{A_{1_\Sigma}} \left(\frac{R_{6340}}{R_{7619}}\right)\left(\frac{I_{7619}}{I_{6340}}\right) \qquad (19)$$

The values for A_{1_Σ} and k_r are given in Table I. In the absence of I_2, the $O_2(^1\Sigma)$ is formed by energy pooling of $O_2(^1\Delta)$

$$O_2(^1\Delta) + O_2(^1\Delta) \xrightarrow{k_9} O_2(^1\Sigma) + O_2(^3\Sigma) \qquad (20)$$

Figure 7 is a plot of I_{7619} versus $\dot{m}_{^1\Delta}^2$, confirming that this relationship holds in the present system.

3. $I(^2P_{1/2})$ EMISSION

The absolute calibration of I^* unfortunately is dependent upon knowing the radiative lifetime ratio of $I(^2P_{1/2})/O_2(^1\Delta)$. The situation is therefore similar to that just described for $O_2(^1\Sigma)$. In the present case, the $[I^*]$ is determined as follows:

$$\frac{[I(^2P_{1/2})]}{[O_2(^1\Delta)]} = \frac{A_{1_\Delta} I_{1.315}}{A_{I^*} I_{1.27}} \cdot \left(\frac{R_{1.27}}{R_{1.315}}\right) \qquad (21)$$

The indicated calibration is made with the Ge detector. The relative response correction is quite small between these two wavelengths. Neither the $O_2(^1\Delta)$ nor the $I(^2P_{1/2})$ radiative lifetimes is known with a high degree of accuracy, although reasonably good evidence supports 3660 sec for $O_2(^1\Delta)$[27] and 0.13 sec for I^*.[30] Throughout this study, the assumed value of $A_{1_\Delta}/A_{I^*} = 3.3 \times 10^{-5}$ was scrutinized for internal consistency with the experimental data.

4. $I(^2P_{3/2})$ RESONANCE FLUORESCENCE

The reaction of HI with excess H atoms was used to generate a known concentration of ground-state iodine atoms:

$$H + HI \rightarrow H_2 + I(^2P_{3/2}) \qquad (22)$$

Even if some of the I atoms recombine to I_2, the reaction

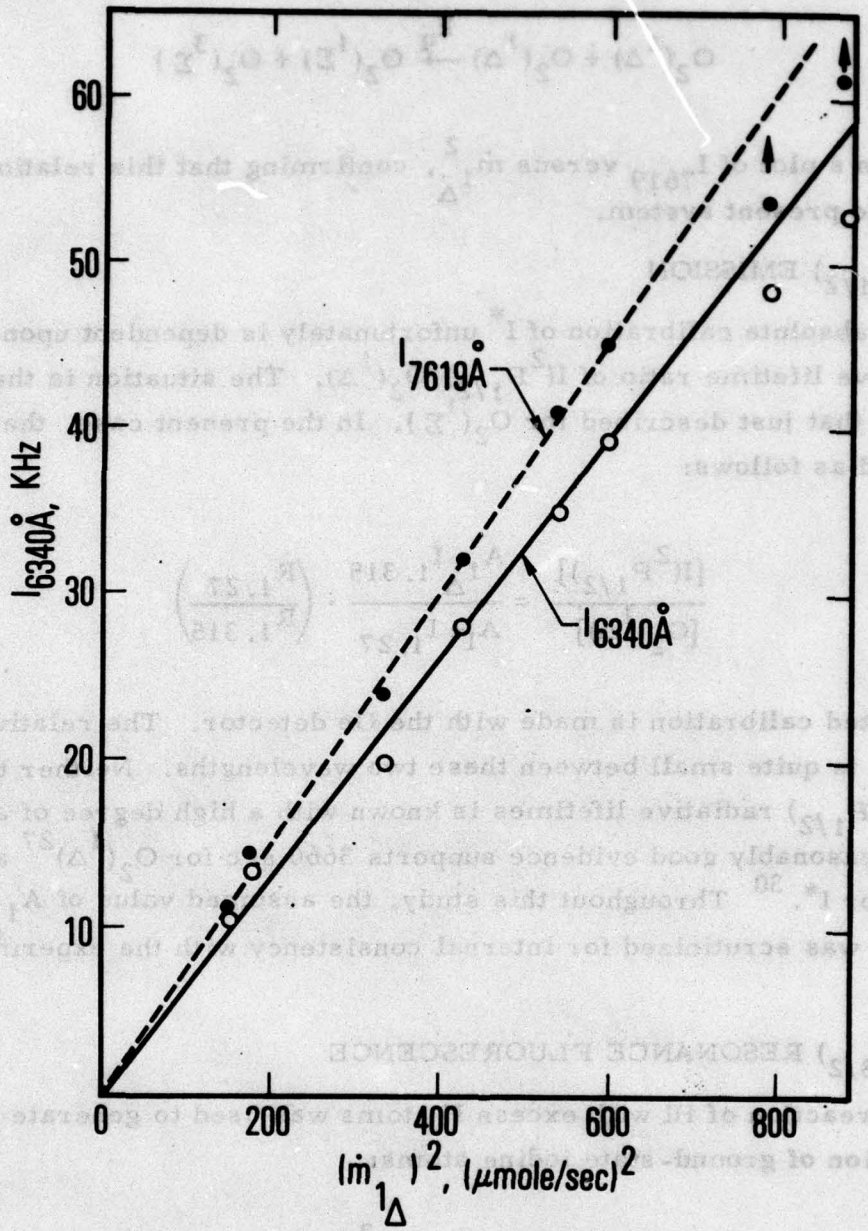

Figure 7. Calibration of 6340-Å "Dimol" Emission and 7619-Å $O_2(^1\Sigma)$ Emission Versus $(\dot{m}_{1_\Delta})^2$

$$H + I_2 \rightarrow HI + I(^2P_{3/2}) \qquad (23)$$

followed by Reaction (22), regenerates them. This titration reaction was used to calibrate atomic resonance fluorescence on the 1830-Å line terminating on $I(^2P_{3/2})$ (Table I). Figure 8 is a plot of the resonance fluorescence intensity versus $[I(^2P_{3/2})] = [HI]_{added}$ and $I_{1830Å}$ versus $[I(^2P_{3/2})] = 2 \cdot [I_2]_{added}$. Since I_2 must be carried in with a diluent gas from a saturator at a known temperature, this plot demonstrates that a well-designed I_2 saturator does allow one to accurately add I_2 to a flow system.

5. I_2 EMISSION

A relative measurement of the $[I_2]$ in the O_2-I_2 system is the intensity of $I_2(B \rightarrow X)$ emission, which has a spectral maximum at 5800 Å.[8] This emission provides the yellow flame observed around the I_2 injector. Since the $B \rightarrow X$ emission is also proportional to $[O_2(^1\Sigma)] \cdot [O_2(^1\Delta)]$,[8] only qualitative conclusions can be drawn about the $[I_2]$ in the system.

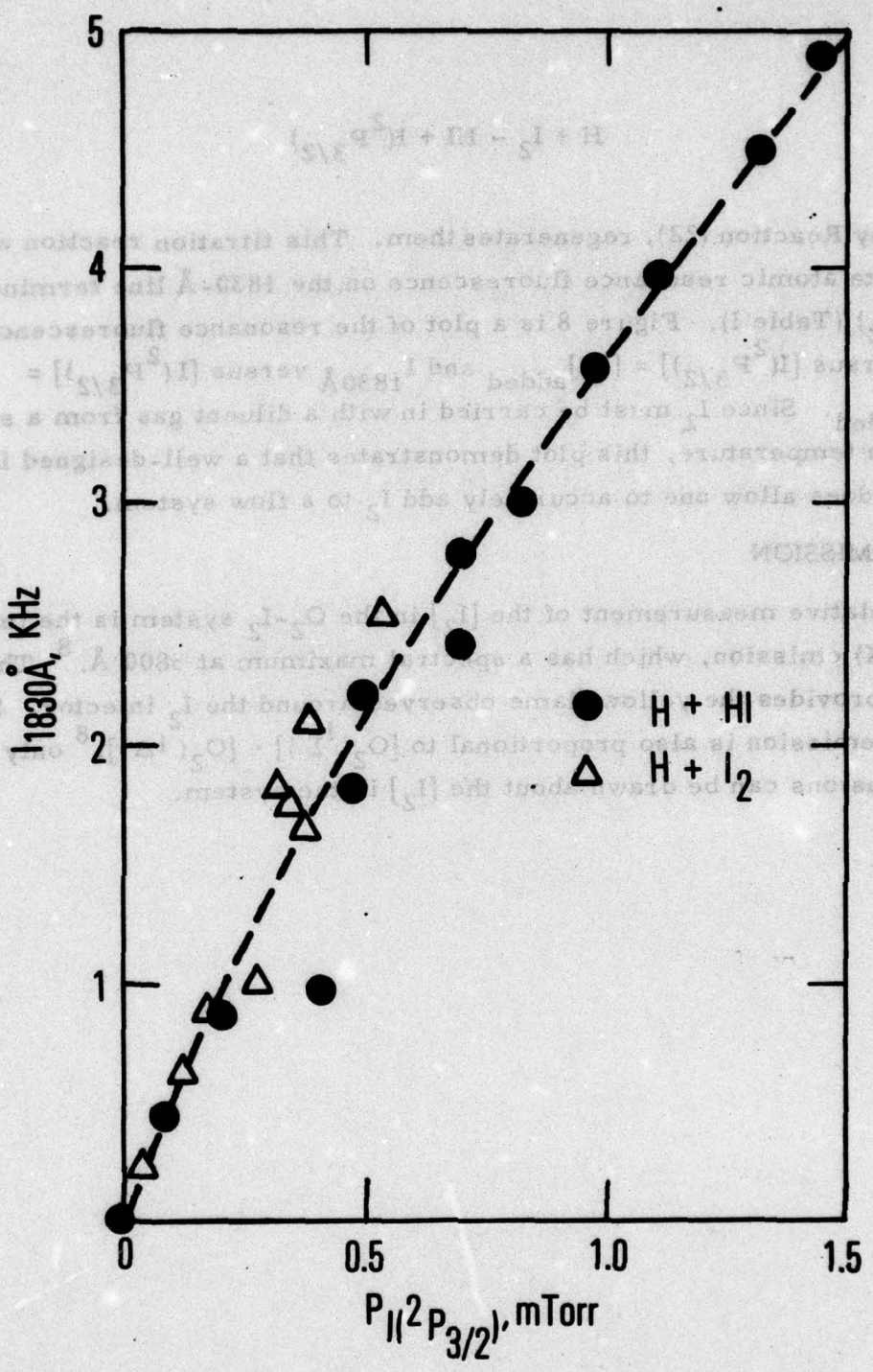

Figure 8. Calibration of Atomic Resonance Fluorescence from $I(^2P_{3/2})$

IV. THEORY OF LOW-TEMPERATURE O_3 PHOTOLYSIS AS SOURCE OF $O_2(^1\Delta)$ AND $O_2(^1\Sigma)$

The photolysis of O_3 was reviewed recently by Lissi and Heicklen.[31] For the case of weak photolysis at low O_3/N_2 ratios, the following mechanism gives a limiting quantum yield of 4 (O_3 molecules destroyed per quantum absorbed):

$$O_3 + h\nu \rightarrow O(^1D) + O_2(^1\Delta) \quad (24)$$

$$O_2(^1\Delta) + O_3 \rightarrow 2O_2 + O(^3P) \quad (25)$$

$$O(^1D) + N_2 \rightarrow O(^3P) + N_2 \quad (26)$$

$$O(^3P) + O_3 \rightarrow 2O_2 \quad (27)$$

This phenomenon might be termed a kinetics-dominated regime, because of the low intensity of photolysis radiation. Large initial concentrations of $O_2(^1\Delta)$ and $O(^1D)$ can be made from the flash photolysis of O_3.[32] During the flash, photolysis dominates the kinetics to a large extent. If the intensity of the flash is such that all the O_3 is removed before kinetics occur, Reactions (25) and (27) are not important. The same criteria also apply to a high-intensity continuous photolysis source. When these criteria are met, the $O(^3P)$ atoms formed in Process (26) are forced to recombine, presumably to ground-state molecular oxygen

$$O(^3P) + O(^3P) + N_2 \rightarrow O_2(^3\Sigma) + N_2 \quad (28)$$

$$O(^3P) + \text{WALL} \rightarrow \tfrac{1}{2} O_2(^3\Sigma) + \text{WALL} \quad (29)$$

The quantum yield of O_3 photolysis is then 1.0, and the $[O_2(^1\Delta)]/[O_2(^3\Sigma)]$ = 2.0.

Continuous photolysis sources are not generally able to dominate the O_3 system kinetics. The $O(^3P)$ and $O_2(^1\Delta)$ compete for the O_3 against the photolysis process. Kurylo et al.[33] measured $k_{25} = 4.5 \times 10^{-11}$ exp (-5620/RT), whereas Davis et al.[34] measured $k_{27} = 2.0 \pm 0.2 \times 10^{-11}$ exp (-4522 ± 210/RT). These two rate coefficients were used to calculate the temperature-dependent first-order destruction rate of O_3 by 1 Torr of $O(^3P)$ atoms and 1 Torr of $O_2(^1\Delta)$ (Table II). These numbers qualitatively indicate the magnitude of the photolysis rate (sec^{-1}) necessary to produce 1 Torr of $O_2(^1\Delta)$ in a cw system without producing excessive $O_2(^3\Sigma)$. The advantage of photolyzing O_3 at low temperatures is immediately clear. Whether low-temperature operation is or is not a necessity depends upon the photolysis rate.

O_3 is especially advantageous as a photolytic precursor for $O_2(^1\Delta)$ because it has a large photon absorption cross section in the ultraviolet ($\sigma = 1 \times 10^{-17}$ cm^2 at 2500 Å)[17] and a large quantum efficiency (>0.95)[35] for the production of $O_2(^1\Delta)$. Our initial photolysis reactor had two Hanovia LL 189A lamps positioned parallel to the photolysis vessel within a MgO-coated elliptical reflector. Approximately 500 W of ultraviolet radiation is emitted by these lamps in sixteen lines falling within the Hartley band of O_3 (200 nm to 320 nm). The final photolysis reactor, which permitted photolysis down to ~ 200 K, had four of the Hanovia LL 189A lamps positioned around a quadruply concentric quartz reaction vessel. The latter apparatus is shown in Figure 9.

Table II. O_3 Reaction Rates with $O(^3P)$ and $O_2(^1\Delta)$ as a Function of Temperature

T,K	k_{25}, cm^3/sec	k_{27}, cm^3/sec	K_{25}, $sec^{-1}/Torr$	K_{27}, $sec^{-1}/Torr$
340	1.1×10^{-14}	2.5×10^{-14}	385	875
320	6.5×10^{-15}	1.6×10^{-14}	228	560
300	3.6×10^{-15}	1.0×10^{-14}	126	350
280	1.8×10^{-15}	5.9×10^{-15}	63	207
260	8.5×10^{-16}	3.2×10^{-15}	29.8	112
240	3.4×10^{-16}	1.5×10^{-15}	11.9	52.5
220	1.2×10^{-16}	6.4×10^{-16}	4.2	22.4
200	3.2×10^{-17}	2.3×10^{-16}	1.1	8.1

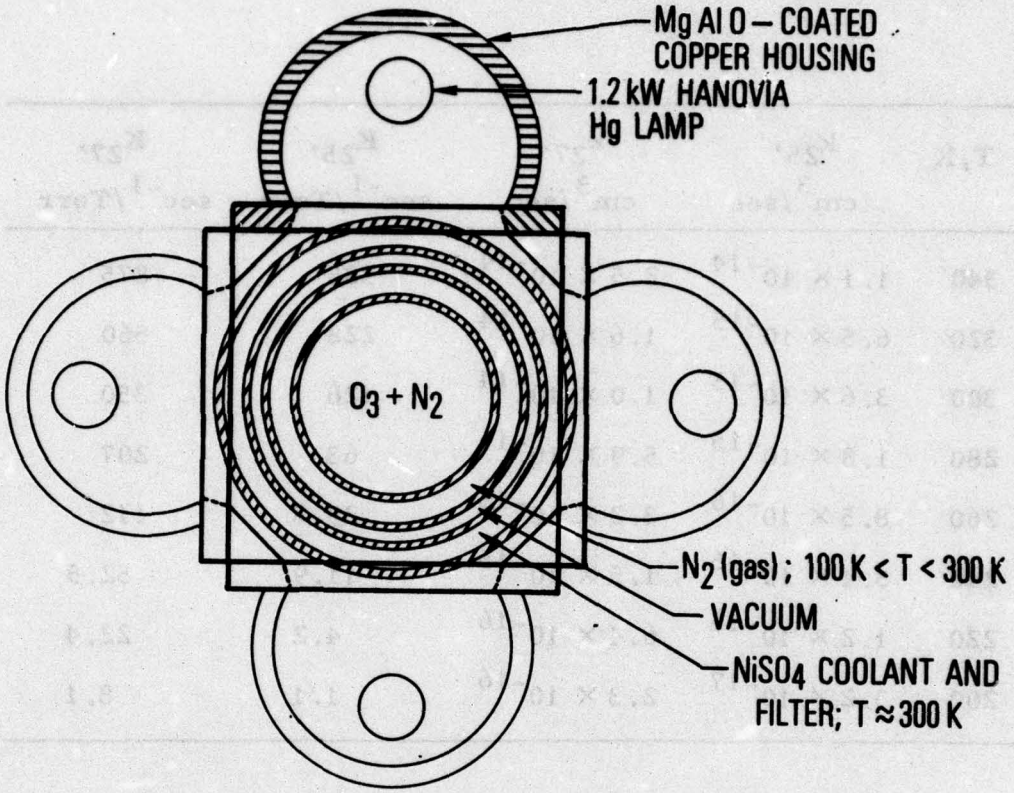

Figure 9. Quadruply Concentric, Low-Temperature O_3 Photolysis Vessel

The photolysis rate, $R(sec^{-1})$, can be expressed in terms of the intensity in each line, $J_i(photons/cm^2\text{-}sec)$, and the O_3 absorption cross section at that line, $\sigma_i(cm^2)$. Thus,[†]

$$R = \sum_i R_1 \approx \sum_i J_1\sigma_i \qquad (30)$$

In this system, R was not measured, although it is perfectly feasible to do so.[36] With the Hanovia specification, the known σ_i for O_3, and a judicious guess for the coupling efficiency of radiation into the photolysis reactor, $R = 10\ sec^{-1}$. At 300 K, this photolysis rate will not be competitive with kinetics when $[O(^3P)]$ and $[O_2(^1\Delta)] > 0.02$ Torr (Table II). For the experiments performed to date, optimum conditions were $[O_3]_{initial} \leq 0.015$ Torr and $[O_2(^1\Delta)] \approx 0.01$ Torr.

For a fixed transit time through the photolysis reactor, the rate of photolysis must be sufficient to decompose virtually all of the O_3, since the remaining O_3 will react with the $O_2(^1\Delta)$. The photolytic removal of O_3 can be written:

$$\frac{-d(O_3)}{dt} = \sum_i \left(\frac{Ji}{L}\right)\left\{1 - \exp[-\sigma_i(O_3)L]\right\} \approx \sum_i J_i\sigma_i(O_3) = R(O_3) \qquad (31)$$

$$\ln \frac{(O_3)_o}{(O_3)} = R\ t \qquad (32)$$

where t is the transit time of the gas through the photolysis region.

[†] In Eq. 30 and in the following analysis, weak absorption of the photolysis radiation is assumed for the sake of clarity. This assumption means replacing Beer's law by $I/I_o \approx 1 - \sigma_i(O_3)L$, where L is the absorption path length. This approximation is valid for all the O_3 densities used in this study.

If 95% of the O_3 has to be photolyzed, Eq. (32) gives $t = 3/R$. With $R = 10\ sec^{-1}$ substitued, $t = 300$ msec. Thus, the residence time in the photolysis vessel must be > 300 msec for complete photolysis, implying a linear flow velocity in the 30-cm-long lamp section of 30 cm/0.3 sec = 1 m/sec. Experimentally, the optimum flow velocity was 1 m/sec.

Although these preliminary calculations fit the data to be presented in Section V quite well, further modelling studies were performed using the The Aerospace Corporation NEST computer program.[37] In this way, it is possible to obtain a more quantitative understanding of the variation of $O_2(^1\Delta)$ with the photolysis rate, R, the $[O_3]$, and with photolysis temperature, T.

The photolysis system was constrained to be isothermal by the artifical addition of a large amount of nondeactivating diluent. Later experimentation showed that for typical conditions ($[O_3]/[N_2] \sim 0.02$), a temperature rise occurs. Thus, the $[O_2(^1\Delta)]/[O_2(^3\Sigma)]$ ratio does not increase as rapidly with temperature decrease as the calculations predict. In addition, the $[O_2(^1\Delta)]$ produced by photolysis is increased by adding SF_6, presumably because of the large heat capacity of the latter molecule.

Figures 10 and 11 are two NEST runs for reasonable experimental conditions. The first case ($P_{O_3} = 0.1$ Torr and T = 300 K) shows that in the absence of other loss processes for $O_2(^1\Delta)$ (such as wall deactivation on these very slow time scales), an $O_2(^1\Delta)/O_2(^3\Sigma)$ ratio of ~ 0.24 would be produced. Photolysis of the same gas mixture at 150 K is predicted to yield $O_2(^1\Delta)/O_2(^3\Sigma) = 1.75$.

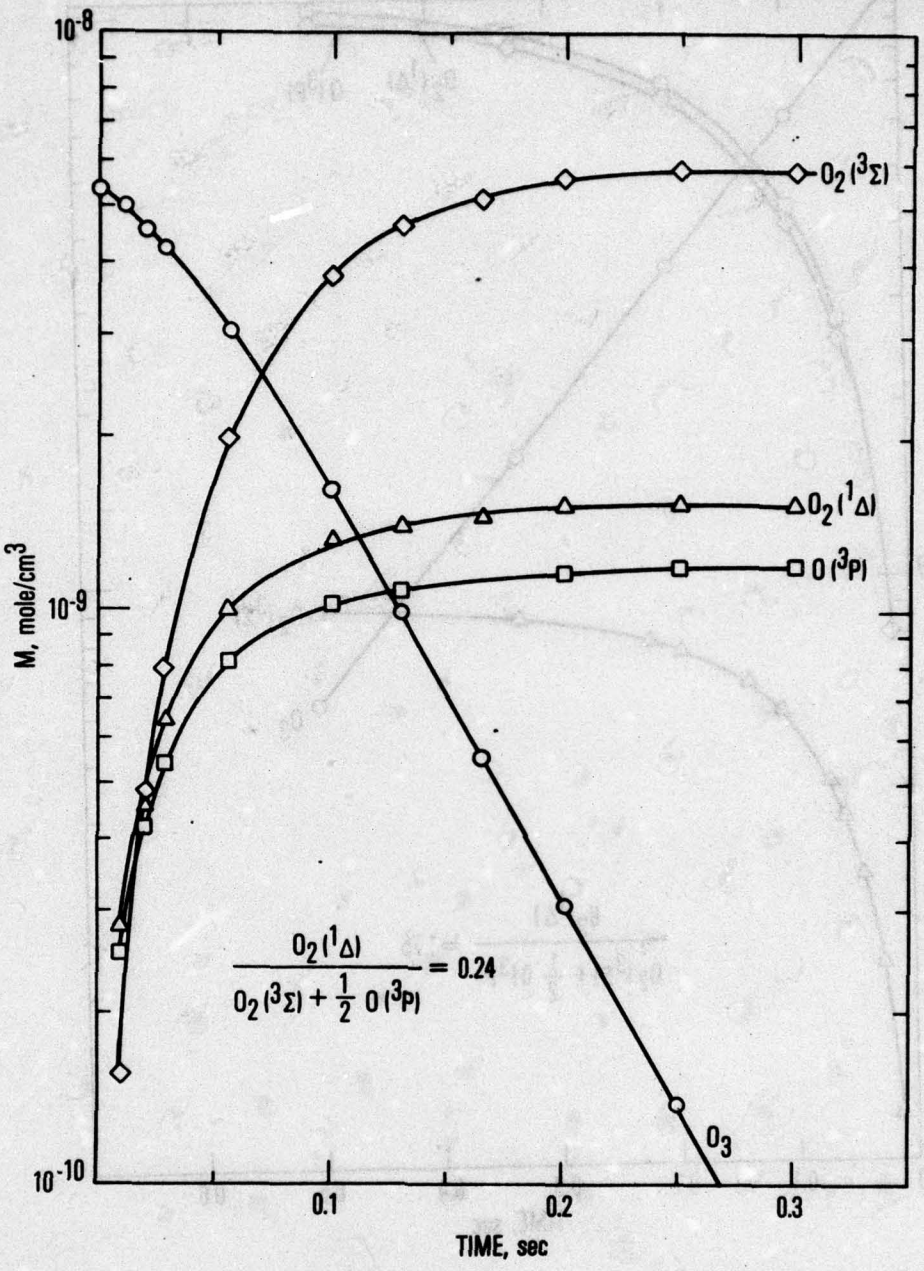

Figure 10. NEST[37] Calculation of $O_2(^1\Delta)/O_2(^3\Sigma)$ Ratio Produced by O_3 Photolysis at T = 300 K. ($[O_3]^0 = 5.4 \times 10^{-9}$ mole/cm^3, P_{N_2} = 5 Torr, R = 10 sec^{-1})

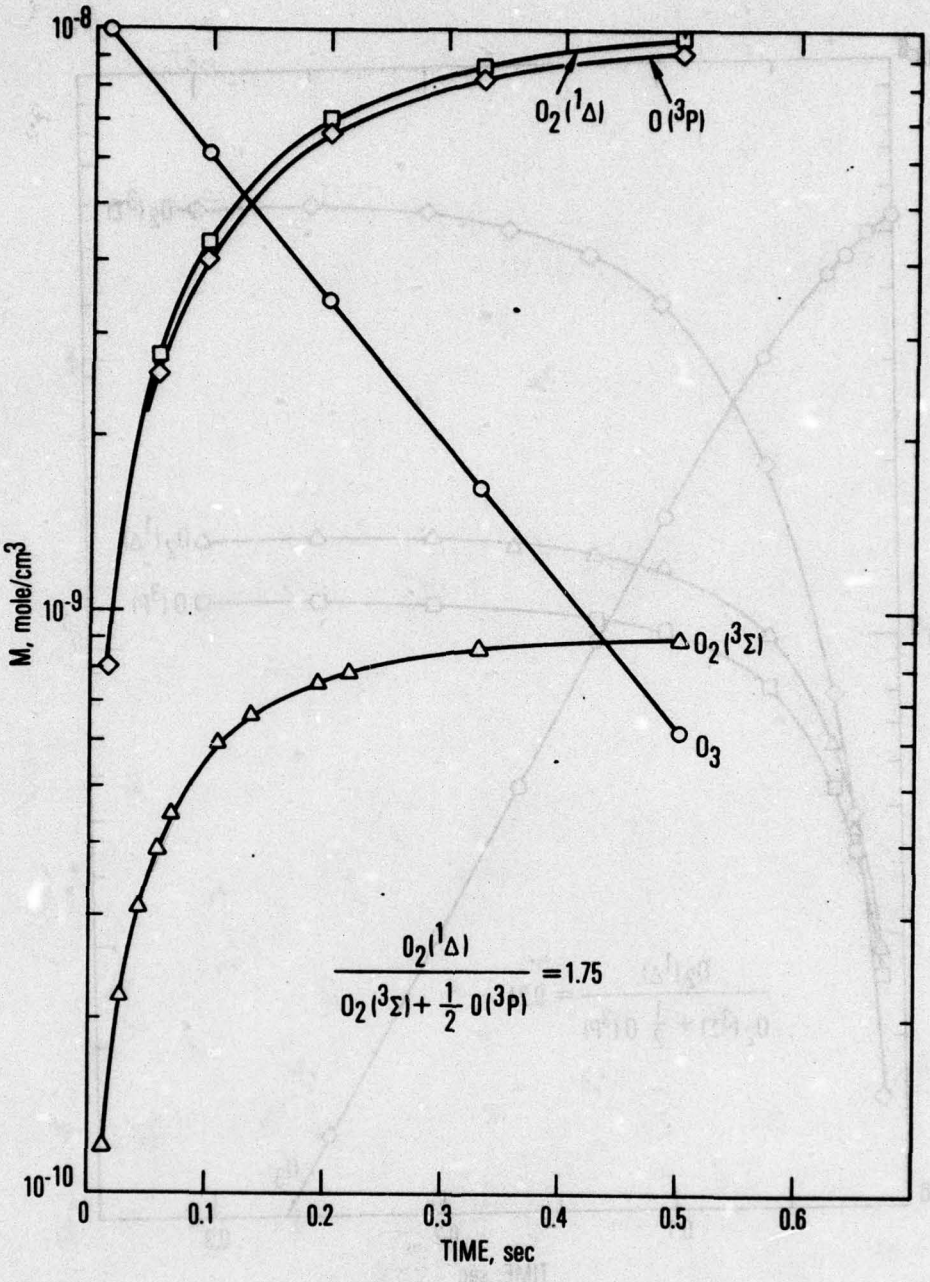

Figure 11. NEST[37] Calculation of $O_2(^1\Delta)/O_2(^3\Sigma)$ Ratio Produced by O_3 Photolysis at T = 150 K. ($[O_3]^0 = 5.4 \times 10^{-9}$ mole/cm^3, P_{N_2} = 5 Torr, R = 10 sec^{-1})

V. RESULTS AND DISCUSSION

A. QUANTITATIVE MEASUREMENTS OF $O_2(^1\Delta)$ AND $O_2(^1\Sigma)$

1. MICROWAVE DISCHARGE EXPERIMENTS

A rather brief parameter study in the 0.5 to 2.0 Torr O_2 pressure range indicated that earlier results[6] obtained with a single 100-W Evenson-type discharge were substantially correct. Figure 12 demonstrates that $O_2(^1\Delta)/O_2(^3\Sigma) \approx 0.07$ is typical of most experimental conditions; Figure 13 indicates a power saturation occuring when the microwave discharge power is raised above 50 W; Figure 14 indicates the variation of $O_2(^1\Delta)/O_2(^3\Sigma)$ with molar flow rate of O_2 at constant pressure. Unfortunately, data were not taken at very low O_2 pressures. Figure 15 shows the very slow decay of $O_2(^1\Delta)$ on a phosphoric acid (H_3PO_4) coated surface. This latter measurement was made because Ogryzlo had indicated that H_3PO_4 was the only surface tested that inhibited I-atom wall recombination. Later, it was learned that Halocarbon wax was far superior to H_3PO_4 in suppressing I-atom recombination. The upstream portion of the flow system is still coated with H_3PO_4 since it is somewhat less efficient than pyrex in deactivating $O_2(^1\Delta)$. The best surface coating is one that will not deactivate $O_2(^1\Sigma)$ or recombine I atoms.

2. O_3 PHOTOLYSIS EXPERIMENTS

By means of the photolysis apparatus shown in Figure 2, O_3 was photolyzed in N_2 buffer gas. The initial results (Figure 16) showed that if the $NiSO_4$ solution filter was allowed to heat up, a substantial decrease in the $O_2(^1\Delta)$ production was observed between 25 and 40°C. This $NiSO_4$ solution is in contact with the outer wall of the 19-mm-o.d. photolysis vessel. Some cooling of the photolysis vessel was then achieved by recirculating the $NiSO_4$ solution through an ice bath. These data are presented as plots of I_{7619}, which is proportional to $[O_2(^1\Delta)]^2$, versus time after the lamps were turned on (Figure 17). The temperature of the photolysis vessel was cycled, and the

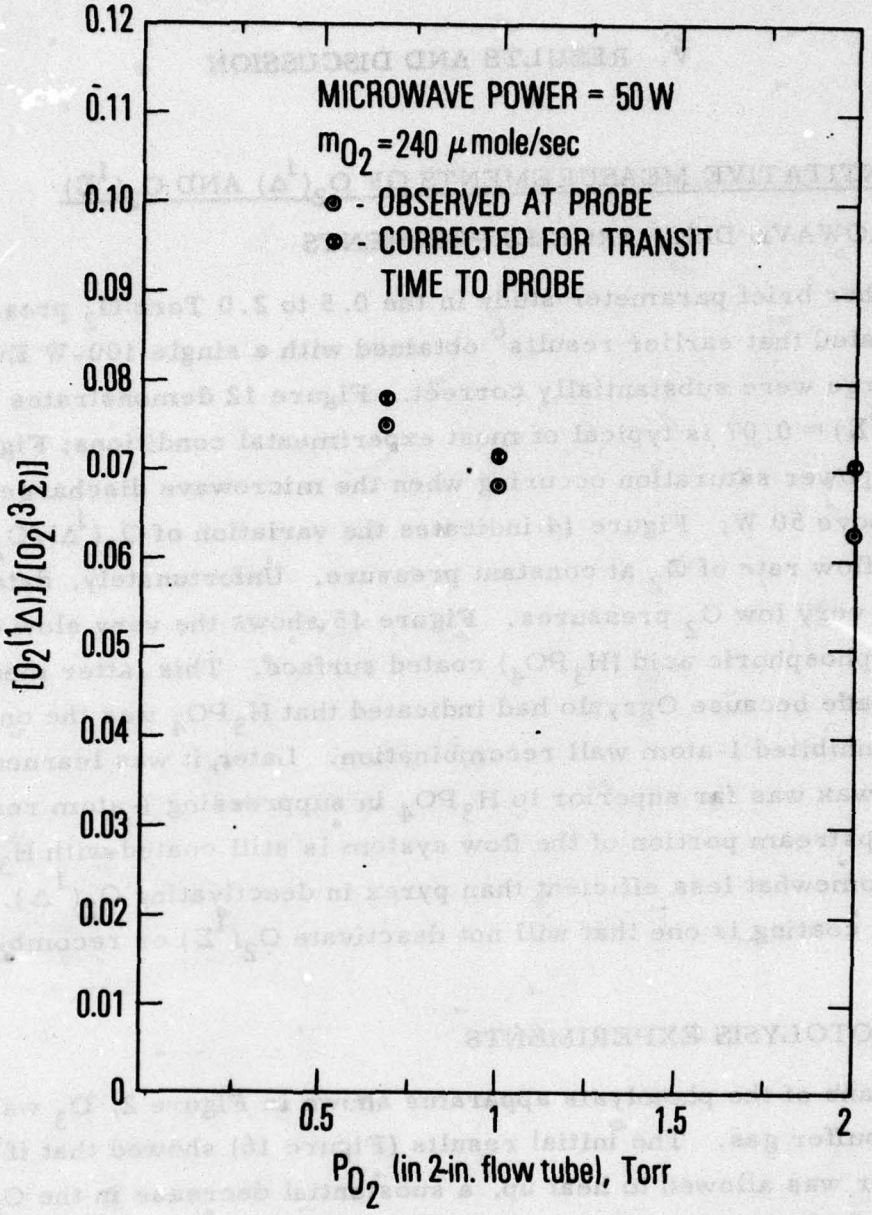

Figure 12. $O_2(^1\Delta)/O_2(^3\Sigma)$ Ratio Produced by Microwave Discharge; Variation with Pressure

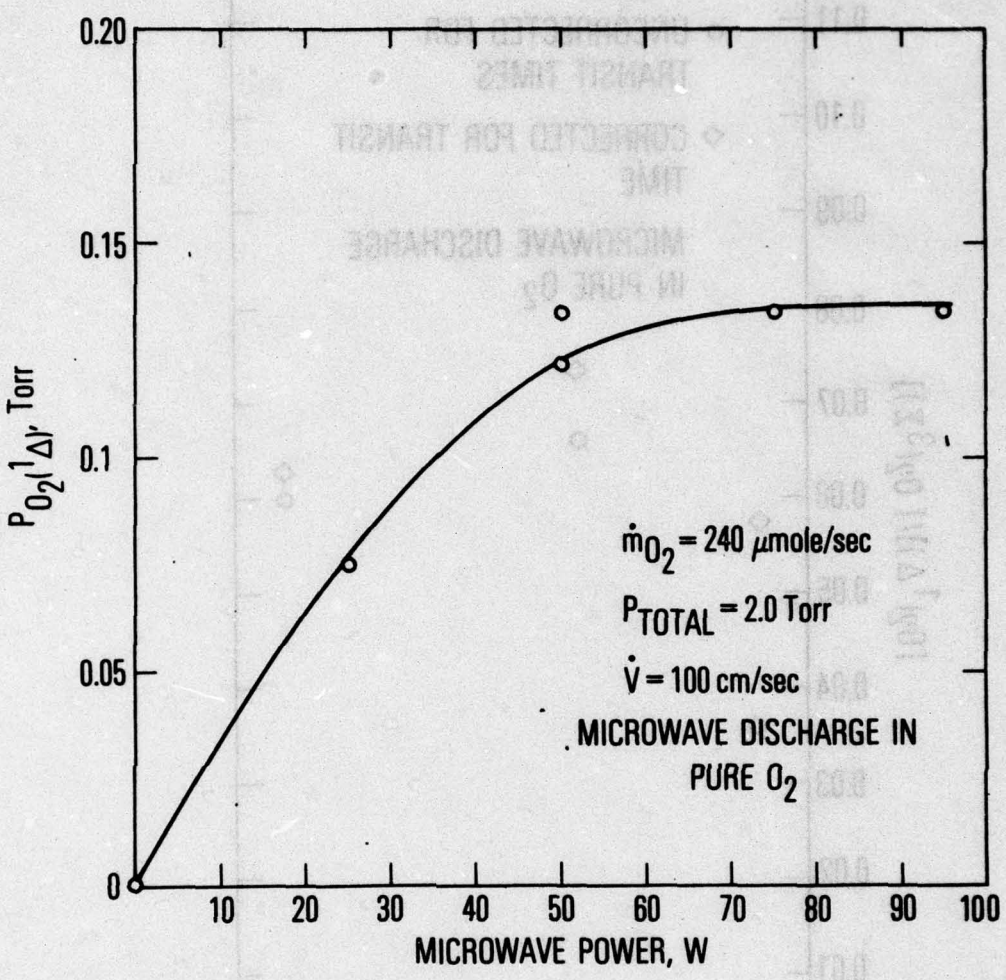

Figure 13. $O_2(^1\Delta)/O_2(^3\Sigma)$ Ratio Produced by Microwave Discharge; Variation with Microwave Power

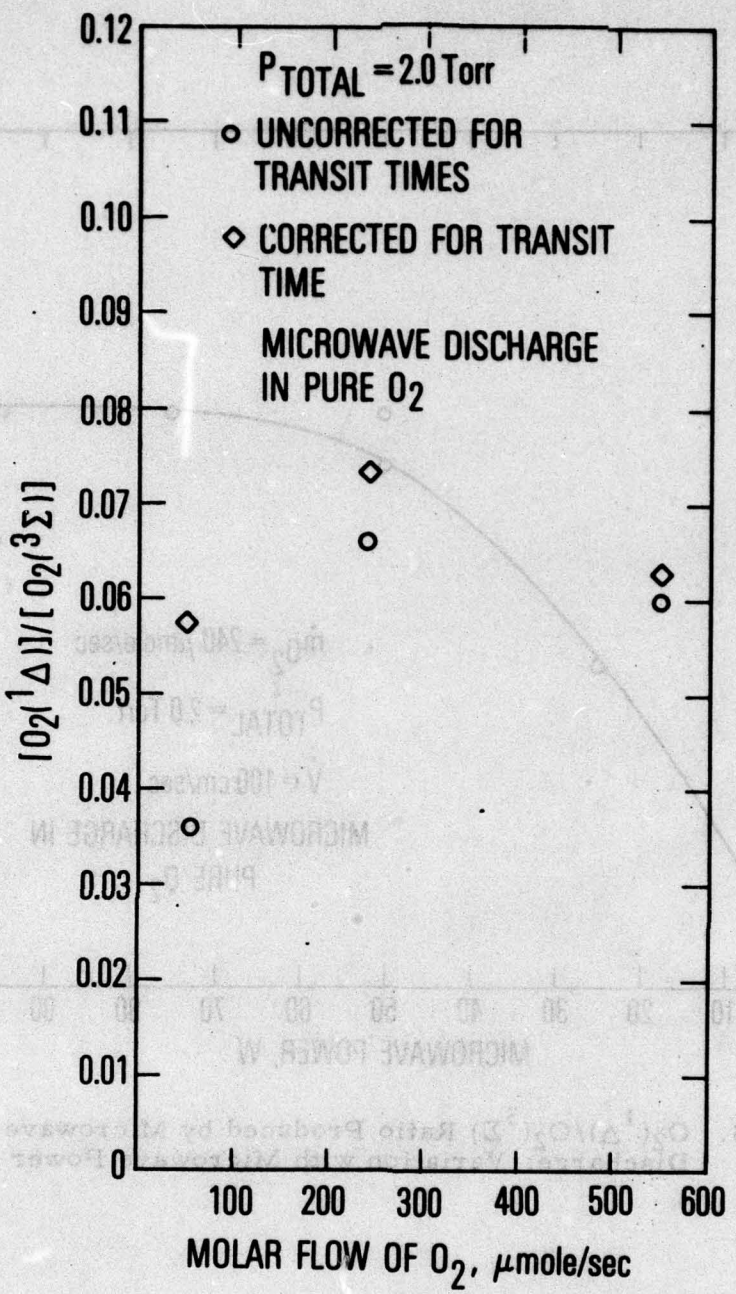

Figure 14. $O_2(^1\Delta)/O_2(^3\Sigma)$ **Ratio Produced by Microwave Discharge; Variation with Molar Flow Rate of** O_2

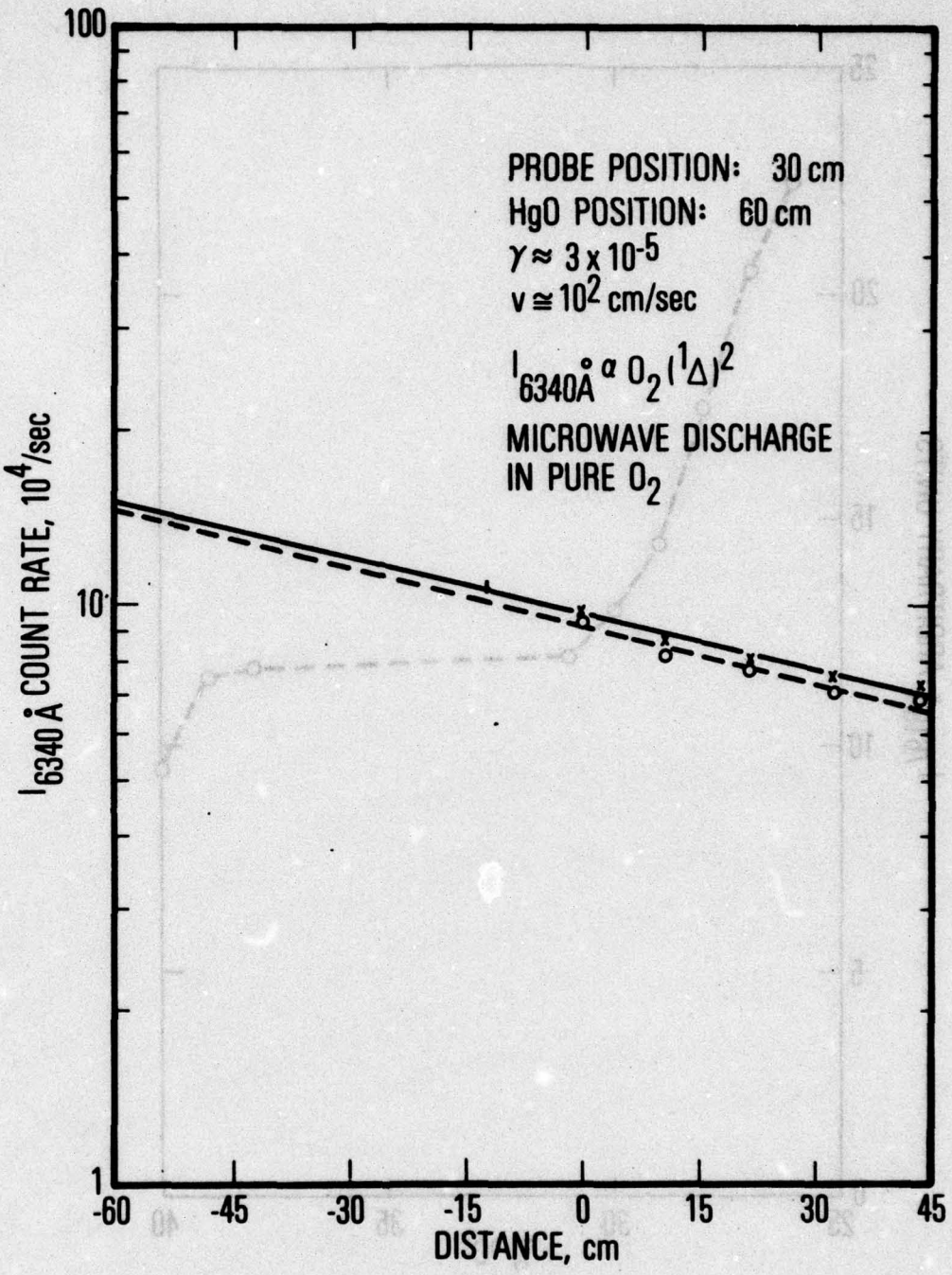

Figure 15. Wall Deactivation of $O_2(^1\Delta)$ in 2-in.-diam Phosphoric-Acid-Coated Pyrex Flow Tube

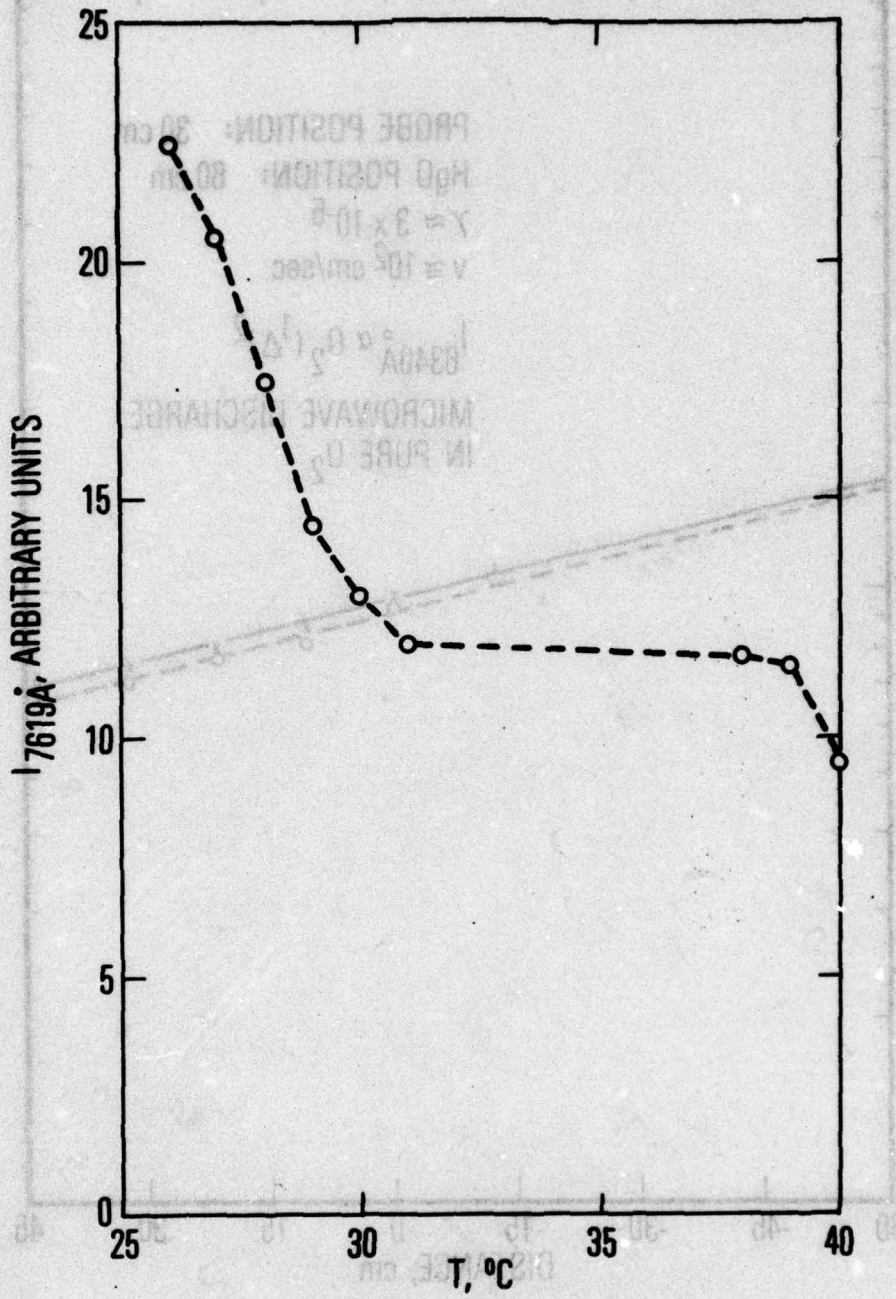

Figure 16. $O_2(^1\Delta)$ Production from O_3 Photolysis at T = 300 to 315 K

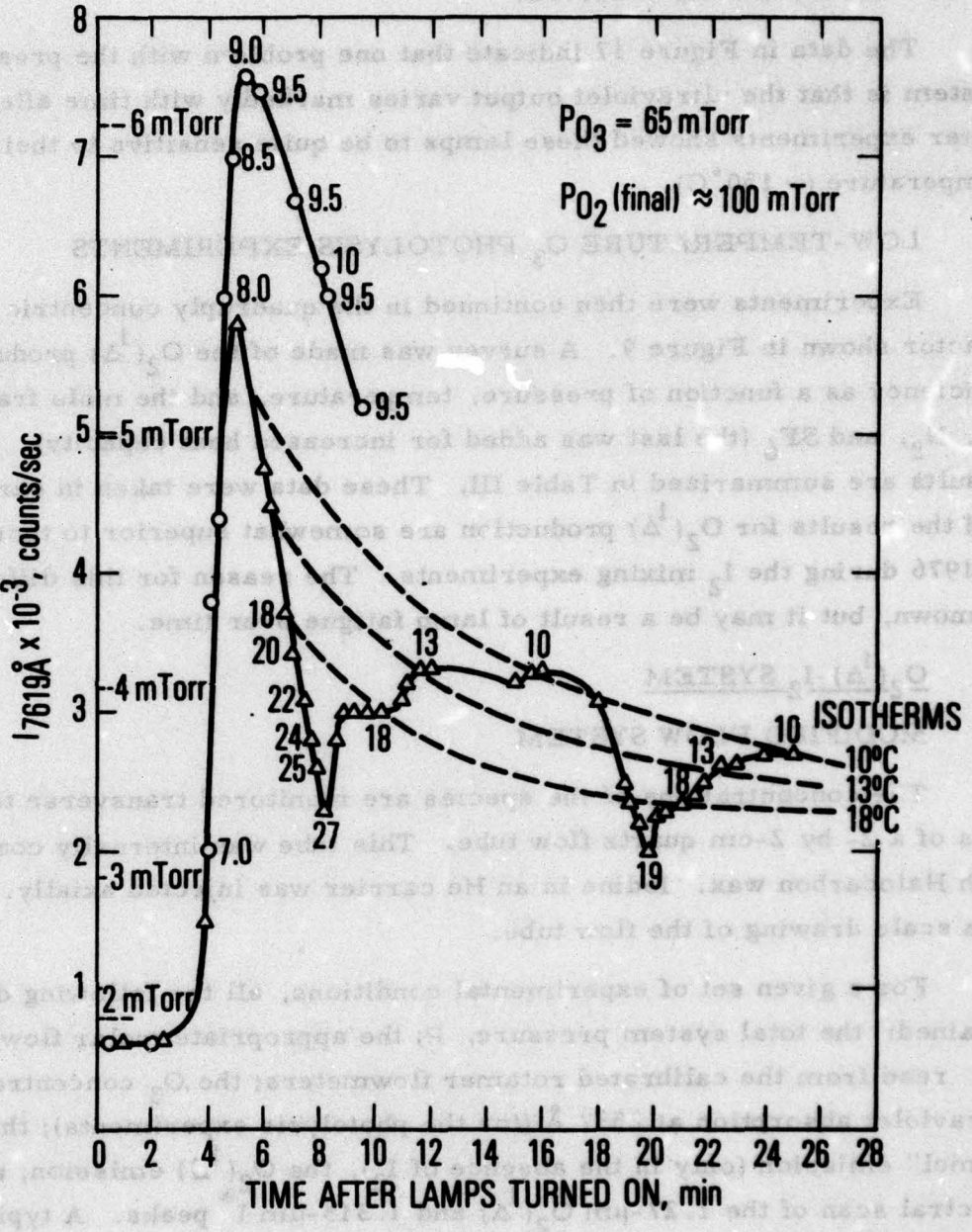

Figure 17. $O_2(^1\Delta)$ Production from O_3 Photolysis at T = 280 to 300 K; Variation with Photolysis Lamp Warm-Up Time

data fall roughly along isotherms. Once again, an improved $O_2(^1\Delta)$ yield at lower temperatures is observed.

The data in Figure 17 indicate that one problem with the present lamp system is that the ultraviolet output varies markedly with time after turn-on. Later experiments showed these lamps to be quite sensitive to their operating temperature (~ 150°C).

3. LOW-TEMPERATURE O_3 PHOTOLYSIS EXPERIMENTS

Experiments were then continued in the quadruply concentric photolysis reactor shown in Figure 9. A survey was made of the $O_2(^1\Delta)$ production efficiency as a function of pressure, temperature, and the mole fractions of O_3, N_2, and SF_6 (the last was added for increased heat capacity). The results are summarized in Table III. These data were taken in early 1975, and the results for $O_2(^1\Delta)$ production are somewhat superior to those obtained in 1976 during the I_2 mixing experiments. The reason for this difference is unknown, but it may be a result of lamp fatigue over time.

B. $O_2(^1\Delta)$-I_2 SYSTEM

1. MODIFIED FLOW SYSTEM

The concentrations of the species are monitored transverse to the flow axis of a 2- by 2-cm quartz flow tube. This tube was internally coated with Halocarbon wax. Iodine in an He carrier was injected axially. Figure 18 is a scale drawing of the flow tube.

For a given set of experimental conditions, all the following data were obtained: the total system pressure, P; the appropriate molar flow rates, $\dot{m}_i$, read from the calibrated rotamer flowmeters; the O_3 concentration with ultraviolet absorption at 2537 Å (for the photolysis experiments); the $O_2(^1\Delta)$ "dimol" emission (only in the absence of I_2), the $O_2(^1\Sigma)$ emission; and a spectral scan of the 1.27-μm $O_2(^1\Delta)$ and 1.315-μm I^* peaks. A typical near-infrared spectrum is shown in Figure 19.

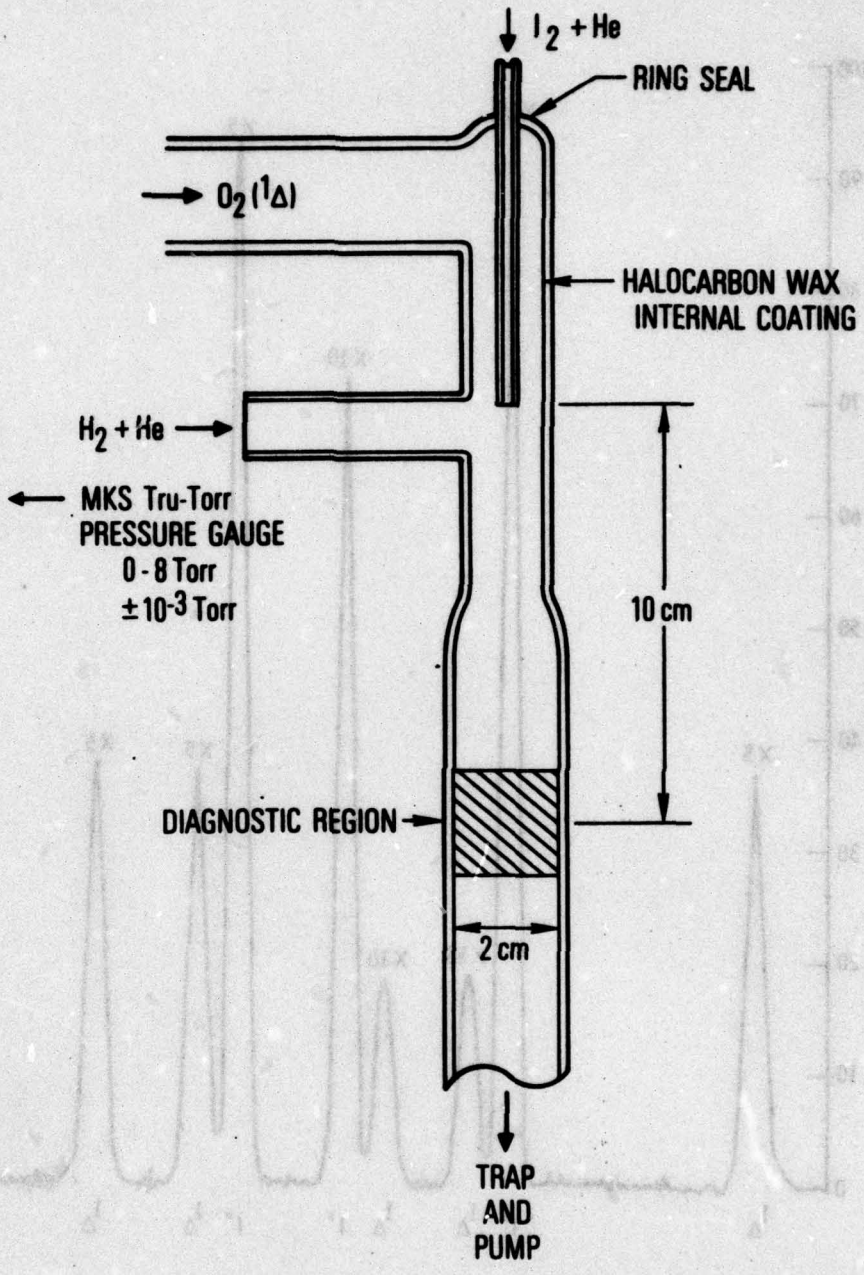

Figure 18. Flow Tube for O_2 + I_2 Experiments

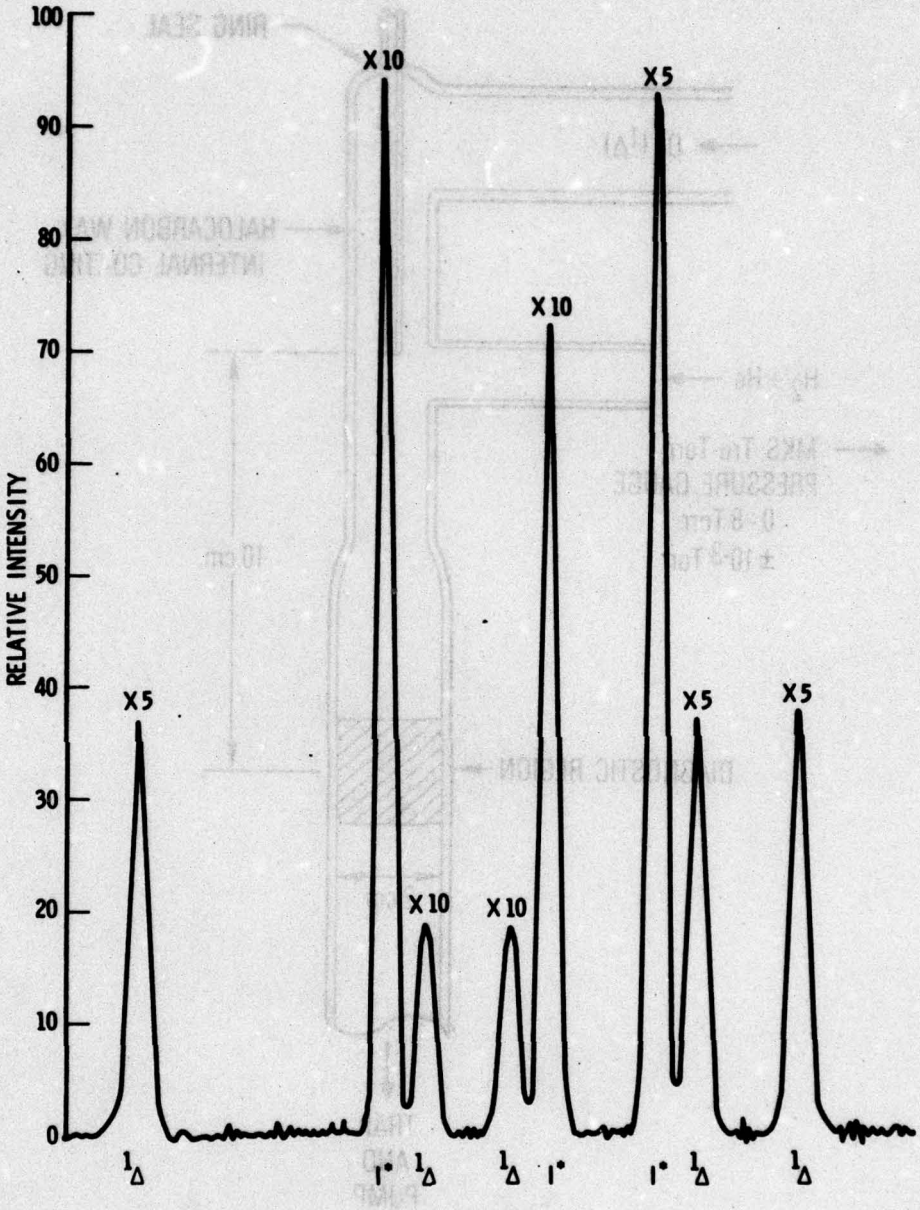

Figure 19. Typical Spectral Scans of 1.27-μm O_2 ($^1\Delta$) Transition and 1.315-μm I-Atom Transition

A small data reduction program was written for the Chemical Kinetics Department of the Aerophysics Laboratory PDP-11 computer to reduce these data to absolute concentrations of the relevant system species.

2. DATA ACQUISITION AND ANALYSIS

The iodine mixing experiments were performed both for discharge-generated and photolysis-generated $O_2(^1\Delta)$. This close comparison of the two $O_2(^1\Delta)$ generation methods is particularly valuable. First, the O_3 photolysis yields the same final products as the discharge; in the present apparatus, O_3 photolysis yields a higher $^1\Delta/^3\Sigma$ ratio, however. Thus, if the O_3 photolysis method can produce a population inversion in the I atom, the discharge method can also, if the criterion $^1\Delta/^3\Sigma > 0.17$ can be met. Second, there is the possibility of a systematic error in determining I^*. By performing the discharge and the photolysis experiments in the same flow system with I_2 added in identical fashion, the relative I^*/I ratios produced by the two methods can be predicted confidently.

The systematic error involves the ratio of the radiative lifetimes of $O_2(^1\Delta)$ and I^*. The $[O_2(^1\Delta)]$ is measured by isothermal calorimetry and the $[O_2(^3\Sigma)]^o$ by a mass flow meter.

$$\dot{m}_{^3\Sigma} = \dot{m}^o_{^3\Sigma} - \dot{m}_{^1\Delta} \qquad \text{(discharge)} \tag{33}$$

$$\dot{m}_{^3\Sigma} = \frac{3}{2}\dot{m}_{O_3} - \dot{m}_{^1\Delta} \qquad \text{(photolysis)} \tag{34}$$

The amount of I_2 added is known (Section III.B.4) and, therefore, with complete dissociation assumed, $[I^*] + [I] = 2\,[I_2]_{added}$ is known. In order to obtain a complete solution to the problem, either $[I^*]$ or $[I]$ must be measured absolutely. Absolute calibration of $[I^*]$ is extremely difficult. In this study, $[I]$ was calibrated absolutely by means of atomic resonance fluorescence in

an O_2-free system, but the technique is awkward to use with O_2 and I_2 present because of the rapidly changing optical transmission of the cell at 1830 Å.

Therefore, there are two choices. The first is to assume the radiative lifetimes of $O_2(^1\Delta)$ and I^* are in the correct ratio:

$$\frac{\Phi_{I^*}}{\Phi_{1_\Delta}} = \frac{A_{I^*}[I^*]\,R_{1.315}}{A_{1_\Delta}[O_2(^1\Delta)]\,R_{1.27}} \tag{35}$$

where Φ is the measured intensity, and R is the black-body calibrated system response (lens, monochromator, and detector) at the indicated wavelengths. All the quantities are measured in the present experiment except $[I^*]$ and (A_{I^*}/A_{1_Δ}).

Therefore,

$$[I^*] = \left(\frac{\Phi_{I^*}}{\Phi_{1_\Delta}}\right)\left(\frac{A_{1_\Delta}}{A_{I^*}}\right)\left(\frac{R_{1.27}}{R_{1.315}}\right)[O_2(^1\Delta)] \tag{36}$$

can be calculated, where $(R_{1.27}/R_{1.315}) = 0.854$ in this system, and the accepted value of $A_{1_\Delta}/A_{I^*} = 3.35 \times 10^{-4}$ (Appendix C). [I] is then determined by mass balance assuming complete dissociation of I_2:

$$[I] = 2\,[I_2]_{added} - [I^*] \tag{37}$$

A second evaluation of $[I^*]$ can be obtained by analyzing Eq.(B-3).

$$\frac{[I^*]}{[I]} = \frac{k_1[O_2(^1\Delta)]}{(k_5 + k_6)[O_2(^3\Sigma)]} \tag{B-3}$$

If the Derwent-Thrush analysis is correct as the present work also indicates, $k_6 \ll k_5$, and the following expression results,

$$[I^*] = K_{EQ}[I]\frac{[O_2(^1\Delta)]}{[O_2(^3\Sigma)]} \tag{38}$$

$$= \frac{2.88(2[I_2]_{added} - [I^*])[O_2(^1\Delta)]}{[O_2(^3\Sigma)]} \tag{39}$$

By the rearrangement of Eq. (39), the following result is obtained:

$$[I^*] = \frac{5.76[I_2]_{added}[O_2(^1\Delta)]}{\left(1 + 2.88[O_2(^1\Delta)]/[O_2(^3\Sigma)]\right)[O_2(^3\Sigma)]} \tag{40}$$

These two methods of analysis are indeed independent, although each of them has assumptions that should be carefully scrutinized. In fact, Derwent and Thrush[7] calculated $A_{I^*} = 6\ sec^{-1}$ by comparison of these two methods. The present experiment suggests that A_{I^*} is somewhat larger than the accepted value of $7.8\ sec^{-1}$.[30] Clearly, it is difficult to control all of the important variables in this system.

As will be shown by the data presented in the following sections, both the discharged O_2 and O_3 photolysis systems behave in a well-understood fashion when small amounts of I_2 are added. When larger amounts of I_2 are added, a catastrophic decrease in $^1\Sigma$ is observed. In this regime, $O_2(^1\Sigma)$ and I^* no longer increase linearly with I_2 addition. The explanation would appear to be that the I_2 is no longer completely dissociated. Since in this data analysis it is assumed that $[I^*] + [I] = 2[I_2]_{added}$, the results cannot be valid after this

assumption breaks down. The presence of substantial amounts of I_2 will also be detrimental to the system since

$$I^* + I_2 \rightarrow I + I_2 \qquad (41)$$

proceeds with a near-gaskinetic rate coefficient. The onset of the $^1\Sigma$ catastrophe appears to be variable but occurs at $[^1\Delta] / [I_2]_{added}$ ratios of ~ 50 to 250 and $[I_2]_{added}$ of 0.2 to 0.5 mTorr. In these multiple-diagnostic experiments, the spectroscopic measurements were not made as a function of mixing time of the I_2 with the $O_2(^1\Delta)$ stream. Therefore, how rapidly (and in what direction) the $O_2(^1\Sigma)$ and $[I^*]$ vary with time is not known. This $^1\Sigma$ catastrophe is semiquantitatively analyzed in the following sections.

3. DISCHARGED O_2: BEHAVIOR OF I^* AND $O_2(^1\Sigma)$

The interrelationship between the extent of I_2 dissociation and the absolute $[O_2(^1\Sigma)]$ must be evaluated. The results of present study confirm the major conclusions of Derwent and Thrush that $O_2(^1\Sigma)$ is responsible for maintaining the dissociation of I_2 (the initial breakup of I_2 in the LTOP experiments is a separate question).

The I_2 dissociation cycle presented in Figure 20 is an example of a positive feedback loop. Any change in the system brings about an accentuation of that change. For example, if the $[I^*]$ decreases, the formation of $O_2(^1\Sigma)$ by k_2 decreases and the dissociation rate of I_2 by k_{15} decreases, thus decreasing the equilibrium amount of $[I^*]$ and $[I]$ still further. If even a small fraction of the $[I_2]_{added}$ remains undissociated, the effect of its gaskinetic quenching efficiency on I^* is a serious problem.

The data to be discussed in this section are shown in Figures 21 through 23. The principal difference in these plots is the $[O_2(^1\Delta)]$ and $[O_2(^1\Sigma)]^0$. Each figure is a plot of Eqs. (B-3) and (B-13).

$$\frac{[I^*]}{[O_2(^1\Delta)]} = \frac{k_1}{(k_5 + k_6)} \frac{[I]}{[O_2(^3\Sigma)]} \qquad (B\text{-}3)$$

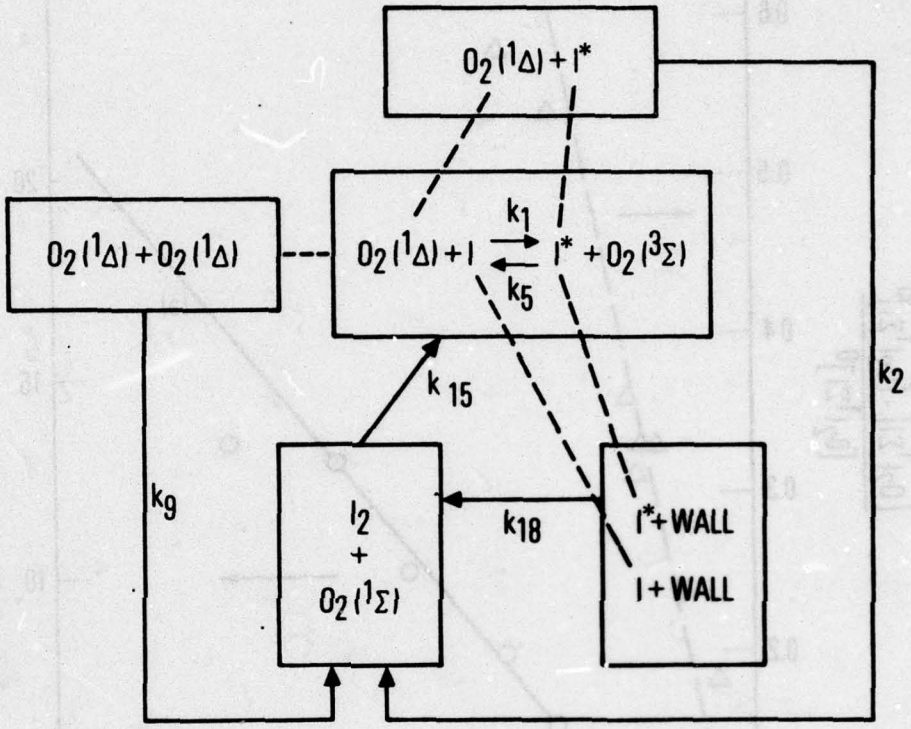

Figure 20. I_2 Dissociation Cycle in $O_2(^1\Delta)$-I Atom Transfer System

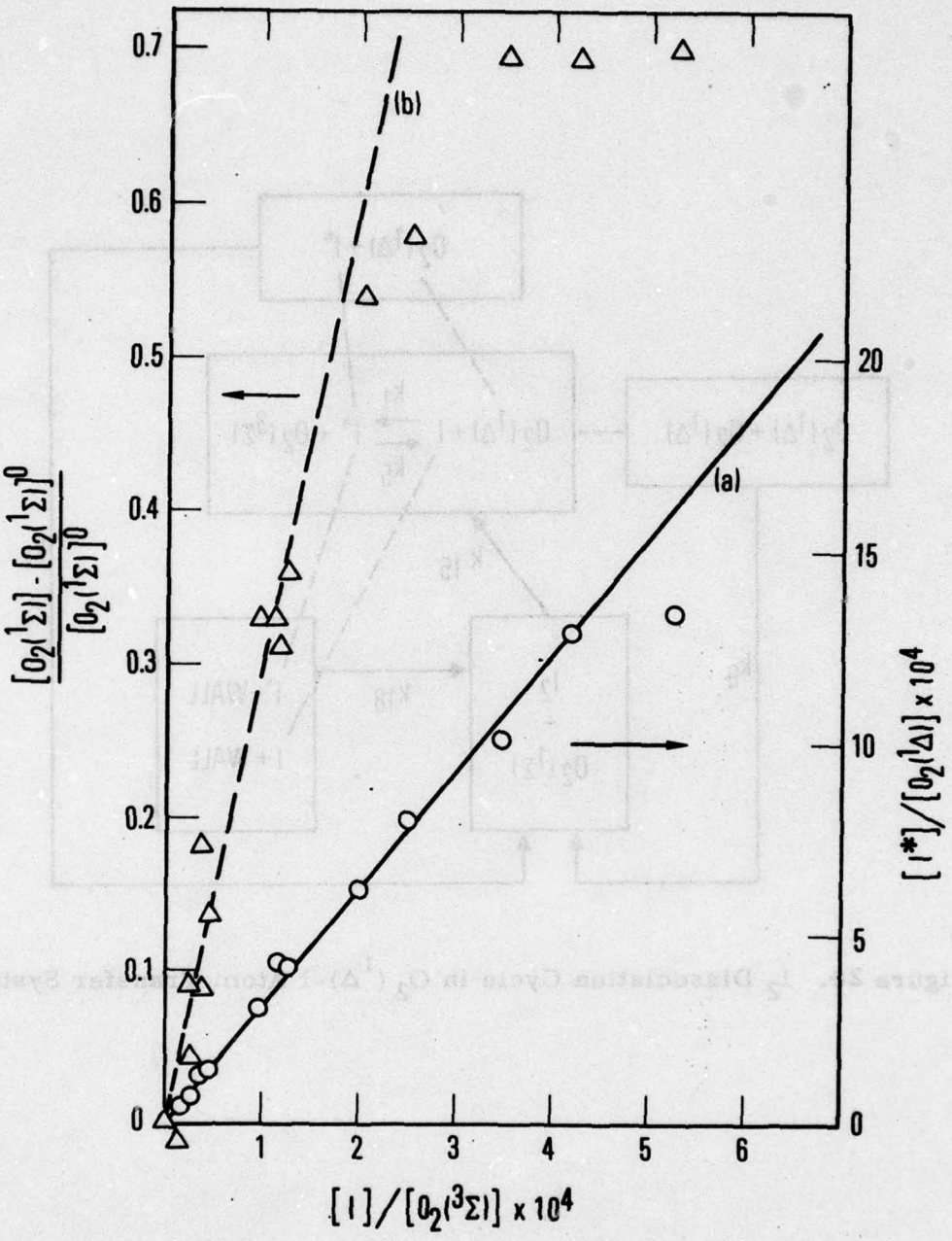

Figure 21. Behavior of I^* and $O_2(^1\Sigma)$ in Discharged O_2. Part I. [Pressures: $O_2(^3\Sigma) = 2.1$ Torr, $O_2(^1\Delta) = 0.162$ Torr, $O_2(^1\Sigma) = 1.18 \times 10^{-4}$ Torr, $(I + I^*)_{max} = 9 \times 10^{-4}$ Torr]

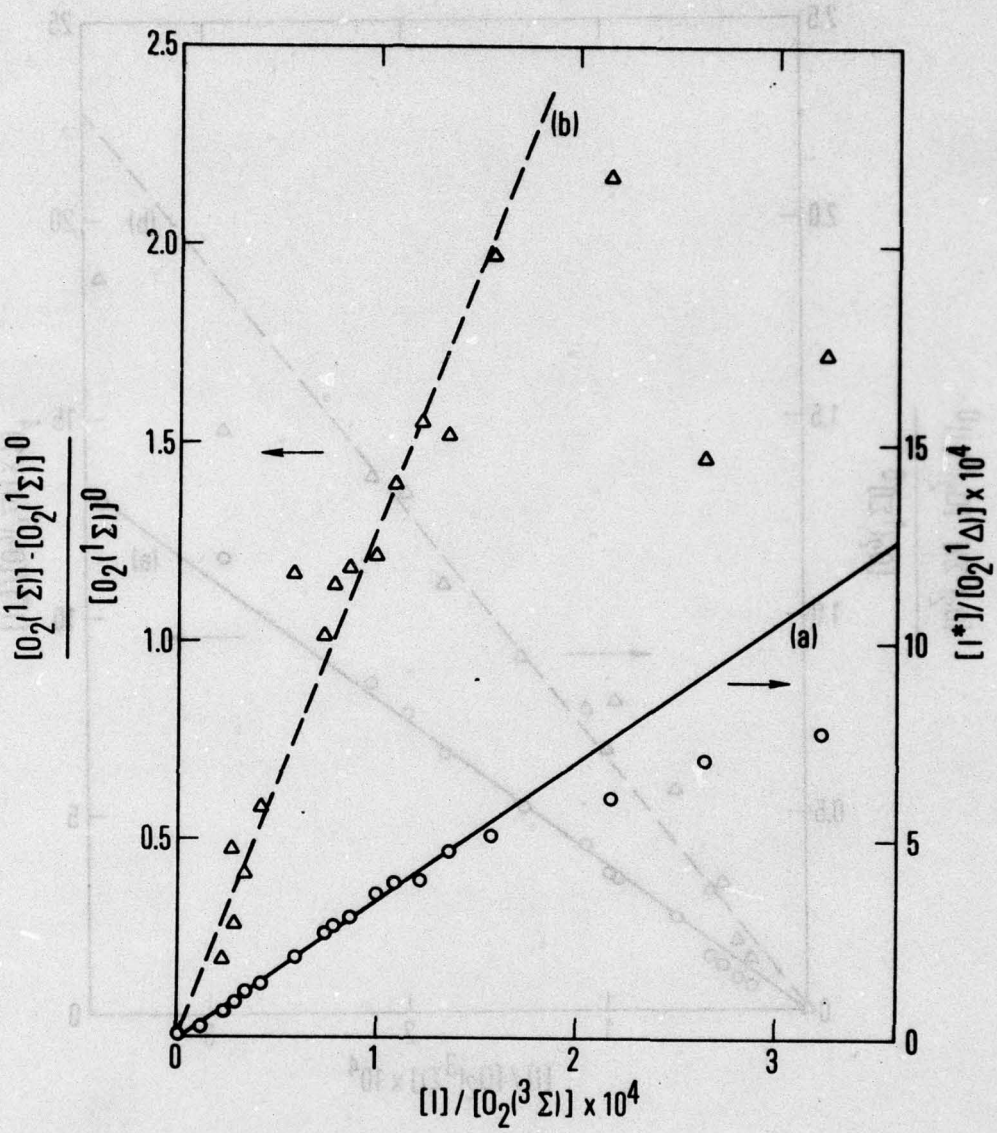

Figure 22. Behavior of I^* and $O_2(^1\Sigma)$ in Discharged O_2. Part II. [Pressures: $O_2(^3\Sigma)$ = 2.2 Torr, $O_2\ ^1\Delta)$ = 0.106 Torr, $O_2(^1\Sigma)$ = 6.9 x 10^{-5} Torr, $(I^* + I)_{max}$ = 6.4 x 10 Torr; $\tau(I_2$ mixing to observation) = 20 msec]

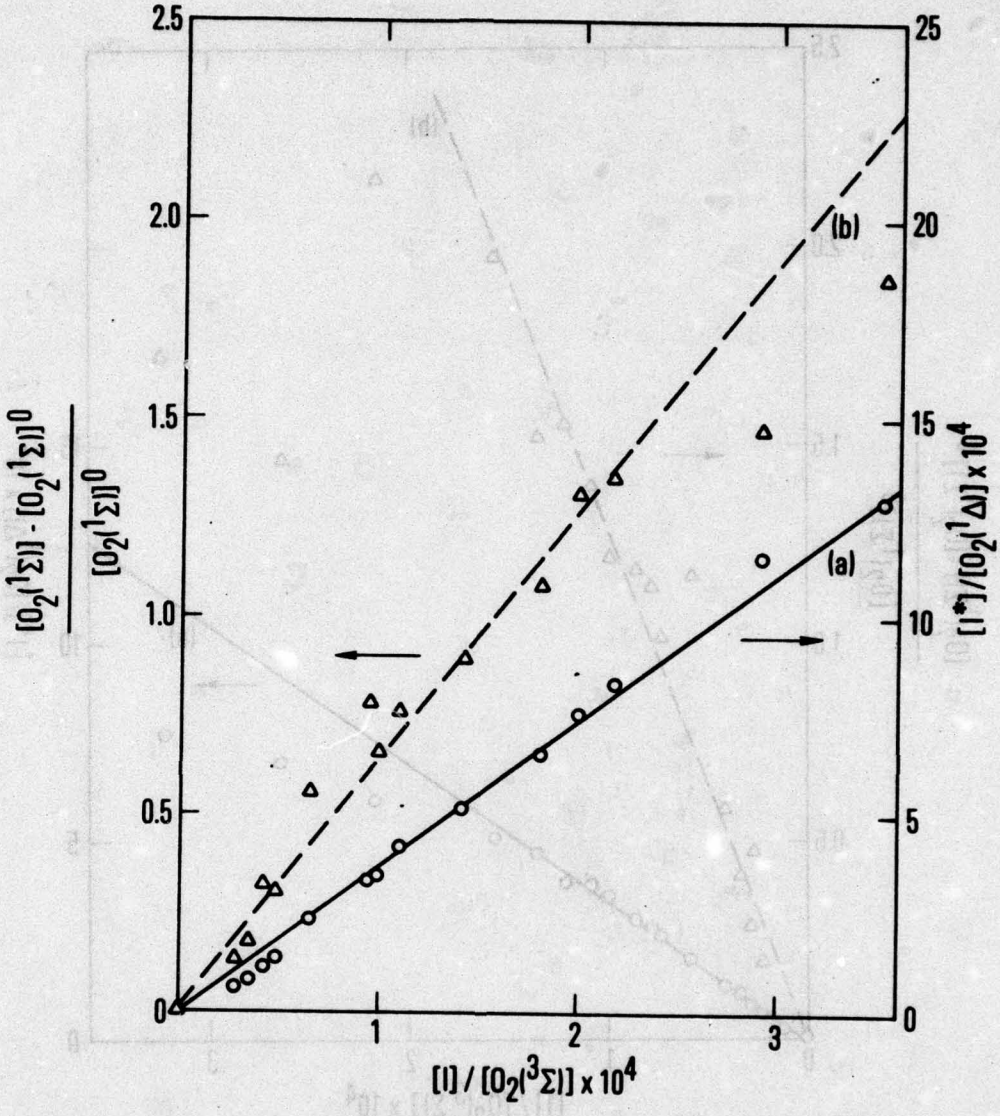

Figure 23. Behavior of I^* and $O_2(^1\Sigma)$ in Discharged O_2. Part III. Pressures $O_2(^3\Sigma)$ = 2.2 Torr, $O_2(^1\Delta)$ = [0.068 Torr; $O_2(^1\Sigma)$ = 1.5×10^{-5} Torr, $(I^* + I)_{max}$ = 6×10^{-4} Torr; $\tau(I_2$ mixing to observation) = 20 msec]

$$\frac{[O_2(^1\Sigma)] - [O_2(^1\Sigma)]^0}{[O_2(^1\Sigma)]^0} = \frac{k_2 k_1}{k_9(k_5 + k_6)} \frac{[I]}{[O_2(^3\Sigma)]} \qquad \text{(B-13)}$$

From Eq. (B-3), a value for the equilibrium constant $K_{EQ} = k_1/k_5 \approx k_1/(k_5 + k_6)$ can be derived. If it is assumed that the $[I_2]$ is known and that it is completely dissociated, a result is obtained for K_{EQ} that is systematically in error by ~ 28%. Subsequent runs gave K_{EQ} values that were somewhat smaller; however, they are uniformly high. This observation can be explained by any combination of the following possibilities:

1. More I_2 is being added than the calibration experiments indicate.
2. A_{*} is too small, Eq. (36).
3. $A_{1_\Delta}^{I^*}$ is too large, Eq. (36).

At high I_2 additions, there is an indication of scaling problems. This is particularly clear for the plot of $[O_2(^1\Sigma)] - [O_2(^1\Sigma)^0]/[O_2(^1\Sigma)]^0$. At low $[O_2(^1\Delta)]$, the scaling also seems to fail for $[I^*]/[O_2(^1\Delta)]$. Some of these deviations may reflect difficulties resulting from our addition of large amounts of He carrier with the I_2. Helium has a large effect on the system gasdynamics (Figure 24). A correction was applied for this effect in the data reduction program; however, in future experiments, Ar instead of He and a heated I_2 saturator should be used to minimize the diluent added with the I_2. Nevertheless, most of the scaling problems result from a more serious source.

Not only does this system exhibit positive feedback, it also can manifest strong spatial inhomogeneities. Such inhomogeneities make kinetic analysis extremely difficult; however, it is easily shown that the centerline of a flow tube will always have the highest ratio of I^*/I. Thus, a laser device is possible in a system where the volume-averaged I^*/I ratio is not inverted.

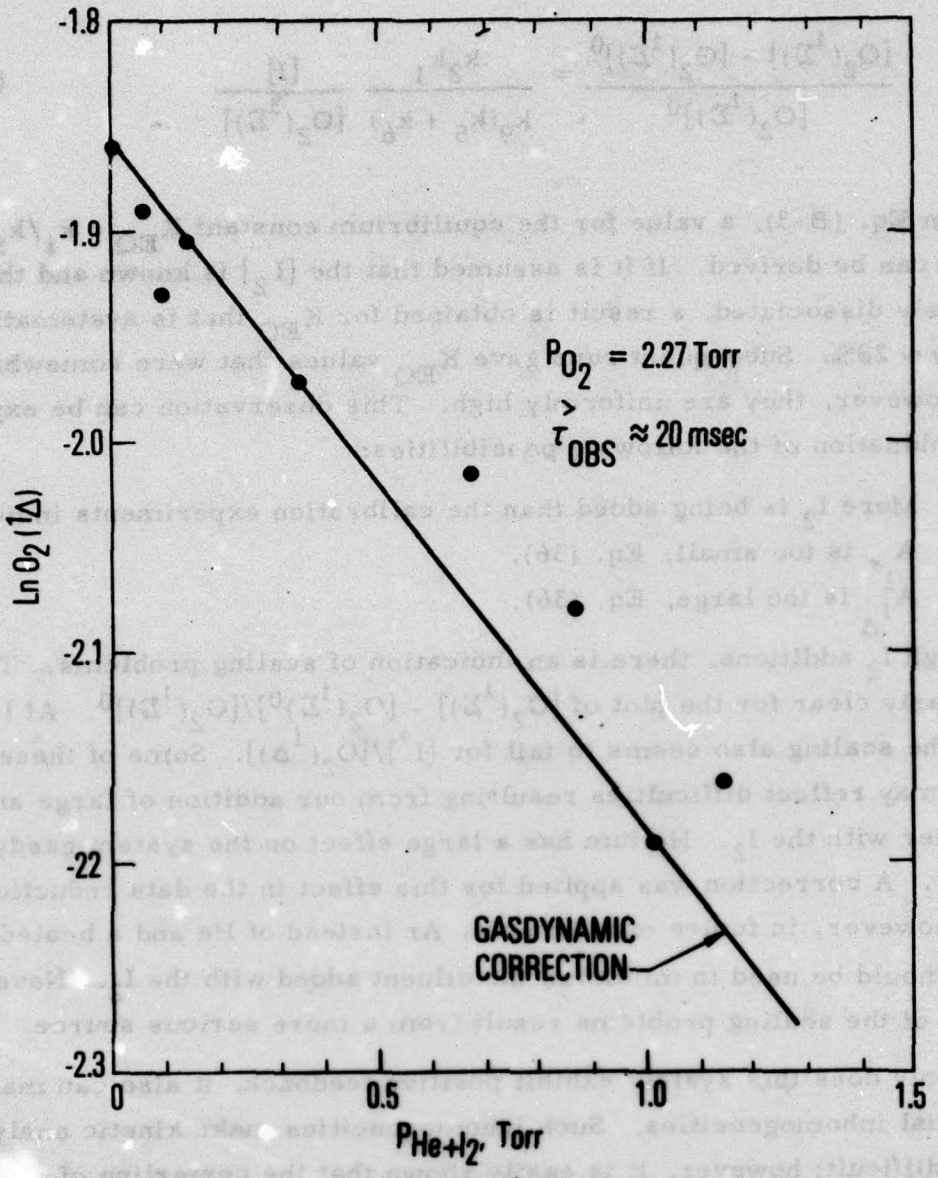

Figure 24. Reduction of $[O_2(^1\Delta)]$ with He + I_2 Addition. (Straight line is gasdynamic effect of He alone.)

In Appendix B, the full steady-state expression for the $[O_2(^1\Sigma)]$ is derived. This equation forcefully demonstrates the effect of inhomogeneous species concentrations

$$\frac{[O_2(^1\Sigma)]}{[O_2(^1\Sigma)]^0} = \frac{1 + k_2 k_1 [I]/k_9(k_5 + k_6)[O_2(^3\Sigma)]}{1 + \left[(k_{15} + k_{16})/k_{10}\right][I_2]} \qquad \text{(B-12)}$$

The second term in the denominator does not appear in the expression derived by Derwent and Thrush, Eq. (B-13), which is a special case for large $[O_2(^1\Sigma)]$ and small $[I_2]_{added}$. In steady-state, I_2 is only formed at the walls by heterogeneous recombination. As I_2 molecules diffuse away from the walls, collisions with $O_2(^1\Sigma)$ dissociate them. Conditions can be found for which I_2 is confined very close to the walls, where $O_2(^1\Sigma)$ will be deactivated in any case (in other words, the boundary conditions for the differential equations are the same). In this case, the flow-tube-averaged emission by $O_2(^1\Sigma)$ obeys the relation given by Derwent and Thrush, and k_2, the $O_2(^1\Delta) - I^*$ energy pooling rate, can be extracted from the plots of Eq. (B-13). What conditions are necessary for this plot to be valid? Primarily, one needs to make $[O_2(^1\Sigma)] \gg [I_2]$ in a large fraction of flow-tube volume. The following conditions help achieve this inequality:

1. Large values of the $[O_2(^1\Delta)]$.
2. Small values of γ_{10} and γ_{18}, the wall deactivation and recombination coefficients of $O_2(^1\Sigma)$ and I atoms, respectively.
3. High system pressures to cut down I-atom and $O_2(^1\Sigma)$ diffusion to the wall and I_2 diffusion away from the wall.

The breakdown of system scaling occurs when the rate of production of $O_2(^1\Sigma)$ molecules in the gas phase can no longer dominate the rate of production of I_2 molecules at the walls. The I_2 molecules then penetrate further

into the gas phase before being dissociated. The conditions for which Eq. (B-13) must be replaced by Eq. (B-12) can be predicted:

$$\frac{k_2 k_1}{k_9(k_5 + k_6)} = 3.8 \times 10^3 \tag{42}$$

$$\frac{k_{15} + k_{16}}{k_{10}} = 1 \times 10^{12} \text{ cm}^3/\text{mol} \; \dagger \tag{43}$$

Therefore, write the following expression:

$$\frac{[O_2(^1\Sigma)]}{[O_2(^1\Sigma)]^0} = \frac{1 + 3.8 \times 10^3 \; [I]/[O_2(^3\Sigma)]}{1 + 1 \times 10^{12} \; [I_2]} \tag{44}$$

If the term $1 \times 10^{12}[I_2]$ approaches 1, deviations from Eq. (B-13) will be observed. For $[I_2] \cong 3 \times 10^{-13}$ mole/cm^3 ($\sim 10^{-5}$ Torr), a 30% deviation is predicted. In Figures 21 through 23, deviations occur for $[I_2]_{added} \cong 1.5 \times 10^{-11}$ mole/cm^3. Thus, if the I_2 were uniformly distributed in the tube, only 2% of the added I_2 would have to remain undissociated to explain the fall-off observed in the present experiments. In addition, the k_2 values determined in our work decrease systematically as $[O_2(^1\Sigma)]^0$ increases. Therefore, even in the "linear regions" of Figures 21 through 23, the term $1 \times 10^{12}[I_2]$ is important. Our value of $k_2 = 1.3 \times 10^{10}$ cm^3/mole-sec, obtained at the highest value of $[O_2(^1\Sigma)]^0$, agrees well with Derwent and Thrush's value of $k_2 = 1.6 \times 10^{10}$ cm^3/mole-sec.

$\dagger$ k_{10} is calculated for a 2-cm-diameter tube, P = 2.5 Torr, and $\gamma_{10} = 0.01$.

If it were possible to start with a large value of $[O_2(^1\Sigma)]^0$, it would be possible to reach a condition where

$$\frac{[O_2(^1\Sigma)]}{[O_2(^1\Sigma)]^0} = \frac{3.8 \times 10^3 [I]}{1 \times 10^{12} [I_2][O_2(^3\Sigma)]} \tag{45}$$

This expression indicates that the fraction of I_2 dissociated remains constant if the $(^1\Sigma)$ remains constant. Thus, $(^1\Sigma)/(^1\Sigma)^0$ could exhibit an extensive plateau region. This plateau will persist until a new I^* quenching mechanism causes a deviation from the equilibrium (k_1, k_5).

After completing this semiquantitative analysis of the behavior of $O_2(^1\Sigma)$, the fraction of the $[I_2]_{added}$ that will be dissociated as a function of radial position in the flow tube must be determined. If it is assumed that I_2 is formed only by wall recombination and that it is dissociated only by $O_2(^1\Sigma)$, steady-state analysis (Appendix B) for the flow-tube averaged $[I_2]$ yields

$$\frac{[I_2]}{[I_2]^0} = \frac{1}{1 + [(k_{15} + k_{16})/k_{18}]\,[O_2(^1\Sigma)]} \tag{B-15}$$

As noted earlier, the amount of undissociated I_2 is inversely proportional to $[O_2(^1\Sigma)]$. The amount of I_2 is also minimized by a small recombination coefficient, k_{18}, for I atoms:

$$k_{18} = \left(\frac{R^2 P}{8 D_o} + \frac{2R}{\gamma_{18} \bar{u}}\right)^{-1} \tag{46}$$

where R is the tube radius, D_o is the diffusion coefficient of I atoms in 1 atm of O_2 ($\sim$0.2 cm^2/sec), P is the pressure in atmospheres, and $\bar{u}$ is the radial velocity of [I]($\approx 1.5 \times 10^4$ cm/sec). Figures 25 and 26 are representative

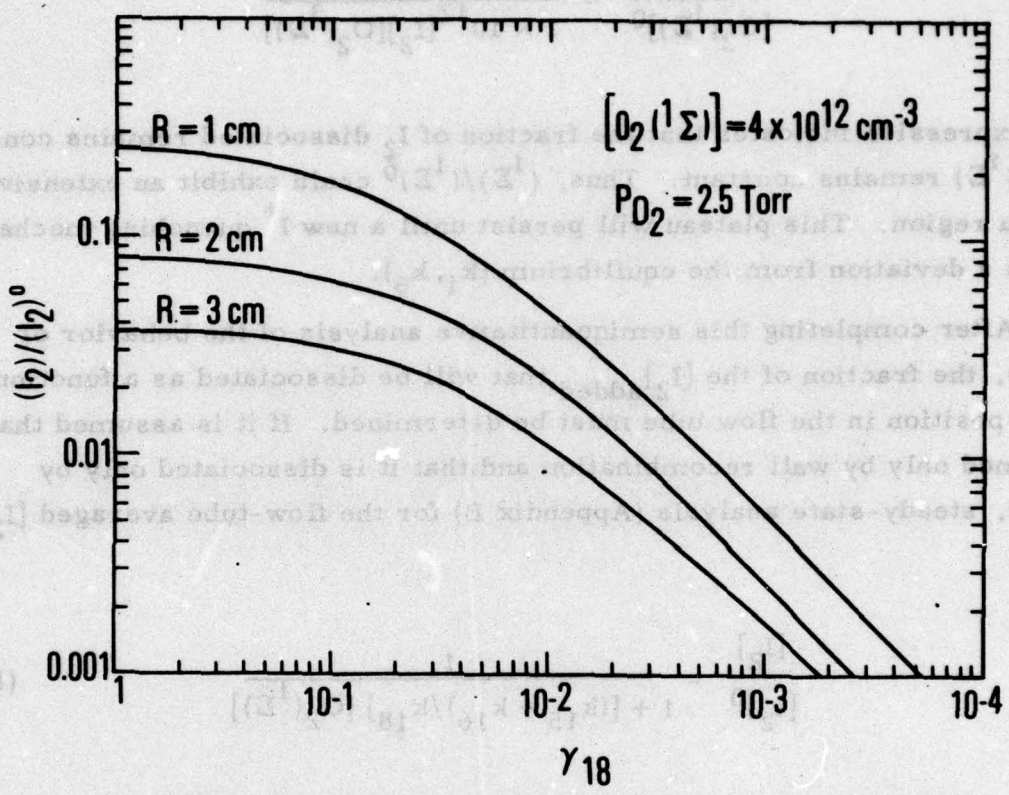

Figure 25. Analytic Prediction of Fractional Dissociation of I_2 by $O_2(^1\Sigma)$. Part I, Variation with Tube Radius (R) and I-Atom Wall Recombination Efficiency (γ_{18}) for $[O_2(^1\Sigma)]$ Typical of Microwave Discharge Conditions

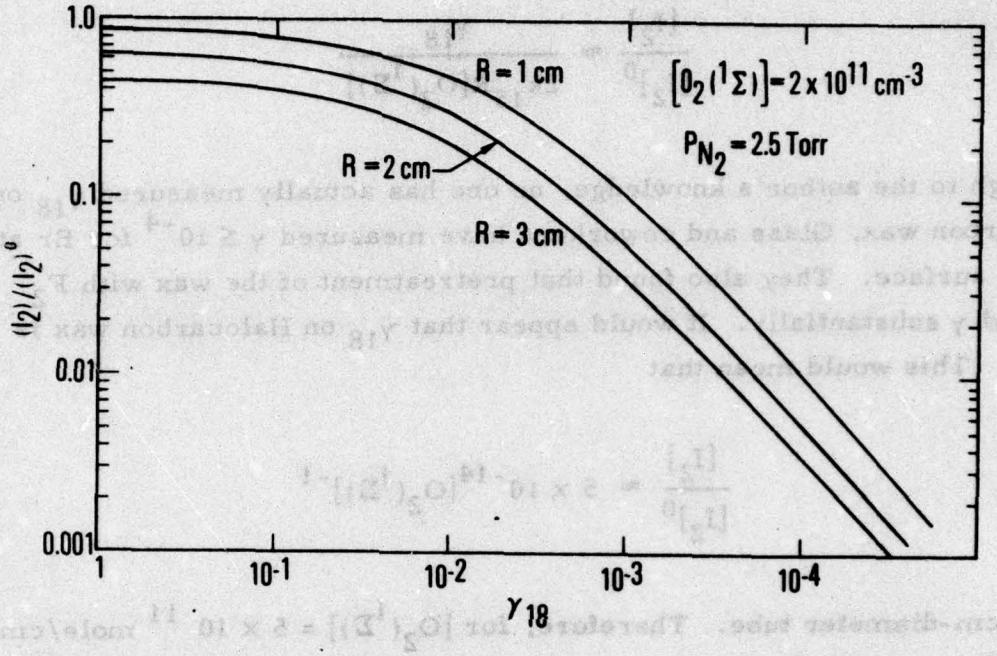

Figure 26. Analytic Prediction of Fractional Dissociation of I_2 by $O_2(^1\Sigma)$. Part II. Variation with Tube Radius (R) and I-Atom Wall Recombination Efficiency for $[O_2(^1\Sigma)]$ Typical of Low-Temperature O_3 Photolysis

plots of $[I_2]/[I_2]^0$ versus γ_{18} for various values of R and $[O_2(^1\Sigma)]$. A linear region of the plots develops when the loss of I atoms is no longer diffusion controlled (i.e., when γ_{18} is small):

$$\frac{[I_2]}{[I_2]^0} \approx \frac{\gamma_{18}}{2k_{15}R[O_2(^1\Sigma)]}$$

Although to the author's knowledge, no one has actually measured γ_{18} on Halocarbon wax, Glass and coworkers have measured $\gamma \leq 10^{-4}$ for Br atoms on this surface. They also found that pretreatment of the wax with F_2 lowered γ substantially. It would appear that γ_{18} on Halocarbon wax is $\simeq 10^{-3}$. This would mean that

$$\frac{[I_2]}{[I_2]^0} \approx 5 \times 10^{-14}[O_2(^1\Sigma)]^{-1}$$

in a 2-cm-diameter tube. Therefore, for $[O_2(^1\Sigma)] = 5 \times 10^{-11}$ mole/cm^3 ($\sim$1 m Torr), only 0.1% of the I_2 would remain undissociated. The highly deleterious effect of an efficiently recombinant surface for I atoms is shown in Figure 27. These are very realistic conditions for discharged O_2 if it is assumed that $\gamma_{18} = 1$ (which is likely for an uncoated surface). Even though 25% of the I_2 remains undissociated, only 1% of the I_2 is undissociated along the tube center, if the $[O_2(^1\Sigma)]$ remains at 4×10^{12}/cm^3.

4. LOW-TEMPERATURE O_3 PHOTOLYSIS: I^* AND $O_2(^1\Sigma)$ BEHAVIOR

An attempt was made to survey the following experimental conditions:

1. $O_2(^1\Delta)/O_2(^3\Sigma)$ ratios of $\sim$0.2 and low concentrations of added I_2.
2. $O_2(^1\Delta)/O_2(^3\Sigma)$ ratios of $\sim$0.2 and high concentrations of added I_2.
3. Maximized $O_2(^1\Delta)/O_2(^3\Sigma)$ ratio and low concentration of added I_2.

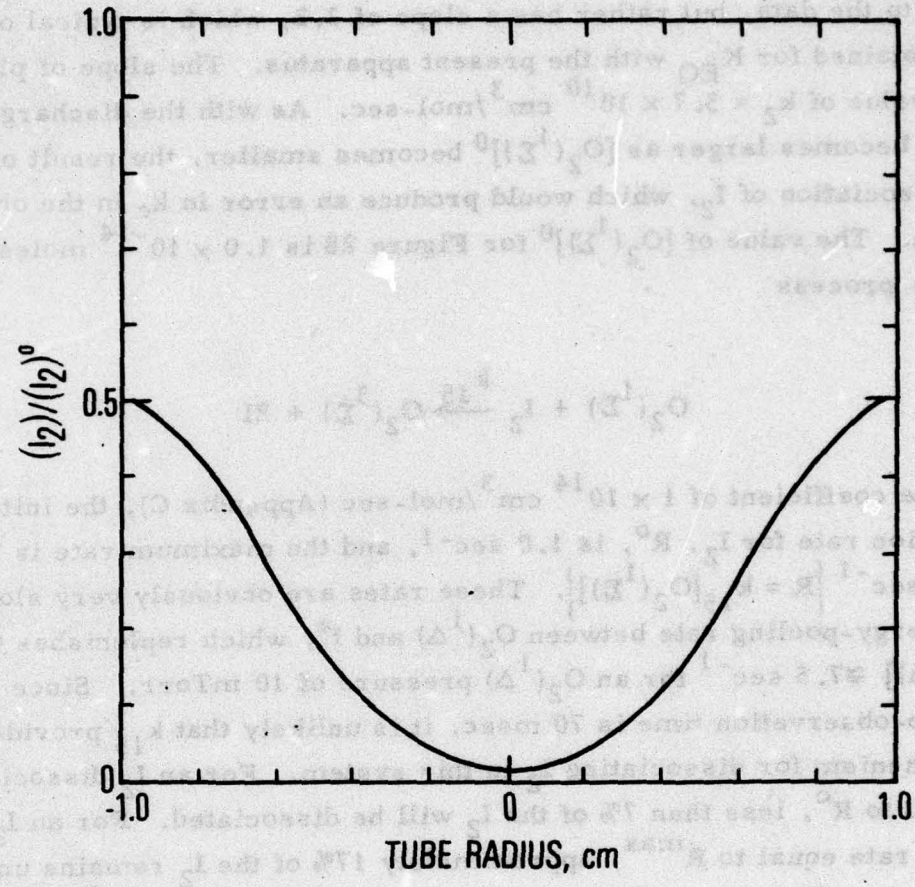

Figure 27. Radial Distribution of I_2 in 2-cm i.d. Flow Tube. Analytic Prediction of the I_2 Fractional Dissociation For a Flow Tube with Efficient ($\gamma_{18} = 1$) Wall Recombination of I Atoms. Experimental Conditions: $P_{O2} = 2.5$ Torr, $[O_2(^1\Sigma)] = 4 \times 10^{12}$ cm^{-3}, $([I_2]/[I_2]^0)_{Ar} = 0.25$

The results for the first case are shown in Figure 28. The [I*]/[I] ratios are ~0.5, i.e., inversion on the 1.315 μm transition. The line (a) is not a fit to the data, but rather has a slope of 3.2, which is typical of the values obtained for K_{EQ} with the present apparatus. The slope of plot (b) gives a value of $k_2 = 3.7 \times 10^{10}$ cm^3/mol-sec. As with the discharged O_2 data, k_2 becomes larger as $[O_2(^1\Sigma)]^0$ becomes smaller, the result of incomplete dissociation of I_2, which would produce an error in k_e in the observed direction. The value of $[O_2(^1\Sigma)]^0$ for Figure 28 is 1.0×10^{-14} moles/cm^3. Since the process

$$O_2(^1\Sigma) + I_2 \xrightarrow{k_{15}} O_2(^3\Sigma) + 2I \qquad (1)$$

has a rate coefficient of 1×10^{14} cm^3/mol-sec (Appendix C), the initial dissociation rate for I_2, R^o, is 1.0 sec^{-1}, and the maximum rate is R^{max} = 20 to 30 sec^{-1} $\left\{R = k_{15}[O_2(^1\Sigma)]\right\}$. These rates are obviously very slow, as is the energy-pooling rate between $O_2(^1\Delta)$ and I^*, which replenishes $O_2(^1\Sigma)$, $k_2[O_2(^1\Delta)] \cong 7.5$ sec^{-1} for an $O_2(^1\Delta)$ pressure of 10 mTorr. Since the I_2 mixing-to-observation time is 70 msec, it is unlikely that k_{15} provides the only mechanism for dissociating I_2 in this system. For an I_2 dissociation rate equal to R^o, less than 7% of the I_2 will be dissociated. For an I_2 dissociation rate equal to R^{max}, approximately 17% of the I_2 remains undissociated at t = 70 msec. Unfortunately, the time evolution of I^* and $O_2(^1\Sigma)$ was not measured. Nevertheless, since $[O_2(^1\Sigma)]^0 \approx 2 \times 10^{-7}$ Torr, $[O(^3P)]$ of 10^{-5} Torr would probably be more effective in producing the initial dissociation of I_2 than is $O_2(^1\Sigma)$. Since those $O(^3P)$ atoms will be consumed, however, for I_2 pressures of 10^{-4} to 10^{-3} Torr, the bulk of the dissociation must be done by $O_2(^1\Sigma)$. The oxygen atoms only serve to initiate the process.

Figure 29 presents data for the second case, where relatively large amounts of I_2 are added. It resembles Figure 28 for small I_2 additions and

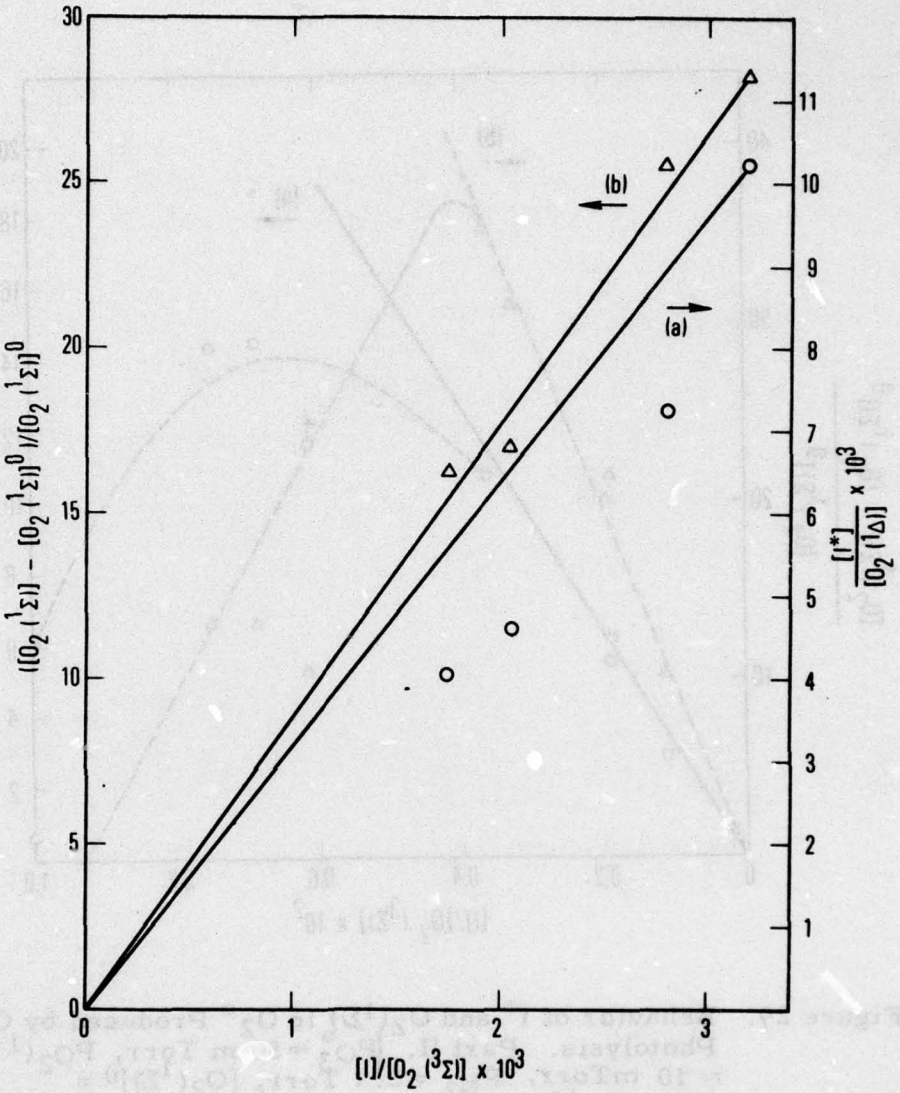

Figure 28. Behavior of I* and $O_2(^1\Sigma)$ in O_2* Produced by O_2 Photolysis. Part I. $P_{O_3}^o \approx 40$ mTorr, $P_{O_2(^1\Delta)} \approx 9$ mTorr, $P_{N_2} = 2.2$ Torr, $[O_2(^1\Sigma)]^o = 1 \times 10^{-14}$ moles/cm^3. From line (a), $K_{EQ} = 3.2$; whereas from line (b), $k_2 = 3.7 \times 10^{10}$ cm^3/mole-sec. $[I^*]/[I] \approx 0.5$

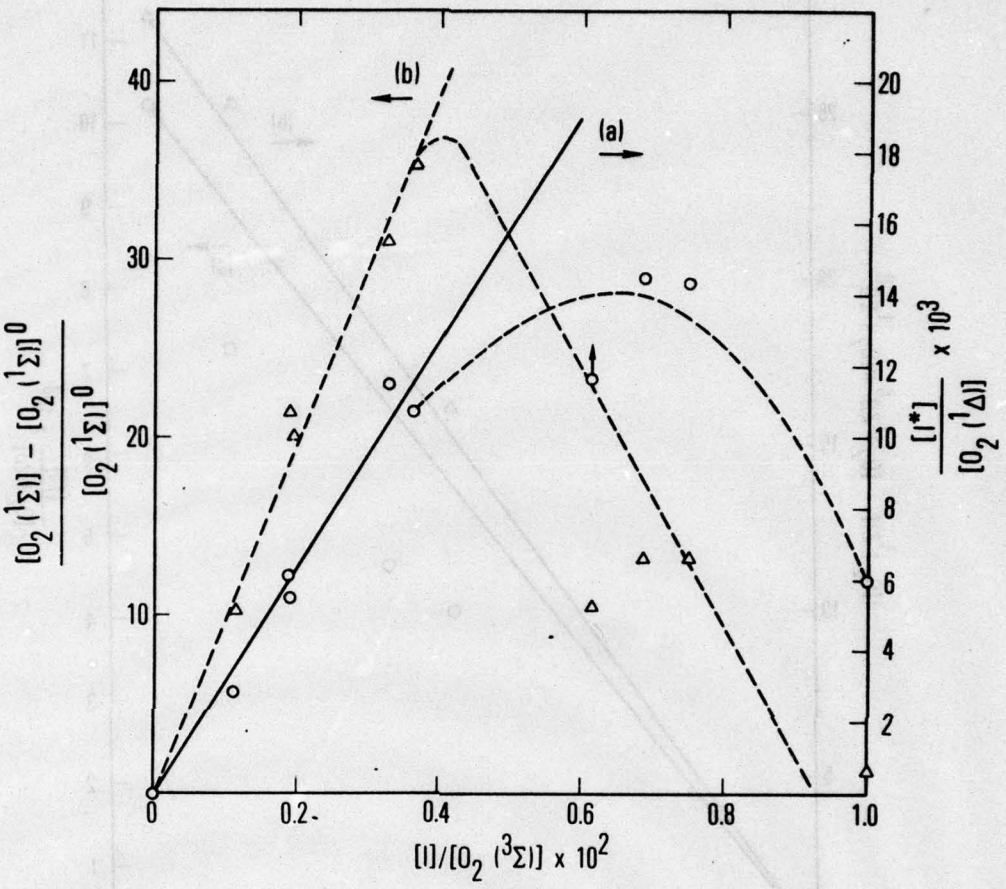

Figure 29. Behavior of I^* and $O_2(^1\Sigma)_o$ in O_2^* Produced by O_3 Photolysis. Part II. $P_{O_3} \approx 50$ m Torr, $P_{O_2(^1\Delta)} \approx 10$ mTorr, $P_{N_2} = 2.1$ Torr, $[O_2(^1\Sigma)]^0 = 1.2 \times 10^{-14}$ moles/cm^3. From line (a), $K_{EQ} = 3.2$; whereas from line (b), $k_2 = 4.1 \times 10^{10}$ cm^3/mol-sec. $[I^*]/[I] \approx 0.5$

then rapidly exhibits the $O_2(^1\Sigma)$ catastrophe for $I^*/O_2(^1\Delta)$ ratios $\geq 1.2 \times 10^{-2}$. Below that ratio, $K_{EQ} = 3.2$ is obeyed, indicating that the I_2 must be nearly dissociated. As in the discharged O_2 case, the gasdynamic corrections are large as a result of the addition of He; thus, the data in region of large I_2 addition are subject to sizable systematic errors. The use of a heated I_2 saturator with Ar as a carrier gas would solve this problem.

For the third case, the optimized production of $O_2(^1\Delta)/O_2(^3\Sigma)$ is presented in Appendix E as a sample calculation. If sufficiently small O_3 concentrations are used, $[I^*]/[I]$ ratios substantially greater than 0.5 can be achieved for very low $[I_2]$ added. Figures 28 and 29 demonstrate that inversion in I^* is possible in the present apparatus only for $[O_2(^1\Delta)] \leq 10$m Torr.

VI. CONCLUSIONS

The low-temperature O_3 photolysis system has permitted us to verify that I^*/I ratios > 0.5 can be produced by energy transfer from $O_2(^1\Delta)$. Thus, a cw energy-transfer iodine laser should be possible to construct. Two results that affect system scaling must be addressed in the future. The first result is from the LTOP experiments, where the initial rate of dissociation of injected I_2 is much too rapid to be explained by the $O_2(^1\Sigma)$ mechanism (k_{15}). In the absence of I_2, $[O_2(^1\Sigma)] = 10^9 - 10^{10}/cm^3$. Even the large dissociation rate of $k_{15} = 2 \times 10^{-10}$ cm^3/mole-sec gives an extremely slow dissociation time $2 \times 10^{-10} \times 10^{10} = 2$ sec^{-1} or $\tau_{Diss} \sim 0.5$ sec. Given the chemical simplicity of this system, the only other species that could be responsible for dissociating I_2 are O_3 and $O(^3P)$. This point really needs to be further clarified since the kinetic modelling cannot reproduce the observed behavior at present.

The second scaling problem that any method of $O_2(^1\Delta)$ production will encounter is the problem of wall deactivation of $O_2(^1\Sigma)$ and wall recombination of I atoms. Basically, the production rate of $O_2(^1\Sigma)$ needs to be large enough to overcome the production rate of I_2 at the walls. This problem can probably be solved with Halocarbon wax coatings. Furthermore, the $O_2(^1\Sigma)$ in the presence of I_2 must be large enough so that the I_2 dissociation time $\{k_{15}[O_2(^1\Sigma)] = \tau_{Diss}\}$ is much shorter than the diffusion time of I_2 from the walls to the tube center. For small diameter systems (≈2 cm), $[O_2(^1\Sigma)] \approx 10^{13}/cm^3$ will be needed.

The low-temperature photolysis method suffers from the low intensity of the present system. Two methods exist for scaling this method to larger cw production rates of $O_2(^1\Delta)$. The first is to use larger and more efficient cw lamps, which are, in fact, available. A less expensive test of the scaling of this method would be to attempt to run quasi-cw by flash photolyzing a sizable volume of $O_3 + N_2 + SF_6$ and flowing the products through

the I_2 mixing region. Given our present knowledge of the ability of the O_3 photolysis system to produce high $O_2(^1\Delta)/O_2(^3\Sigma)$ ratios, this would seem to be a reasonable near-term attempt to reach threshold densities of $[I^*] \sim 1/2[I]$ while awaiting the development of a "clean" chemical generator of $O_2(^1\Delta)$.

REFERENCES

1. J. V. V. Kasper and G. C. Pimentel, "Atomic Iodine Photodissociation Laser," Appl. Phys. Lett. 5, 231 (1964).

2. H. Hohla and K. L. Kompa, "The Photochemical Iodine Laser," in Handbook of Chemical Lasers, R. W. F. Gross and J. F. Bott, eds., Wiley-Interscience, New York (1976).

3. R. W. F. Gross, "High Power Iodine Lasers for Fusion Applications," in Laser-Induced Fusion and X-Ray Laser Studies, S. F. Jacobs et al., eds, Addison-Wesley, Reading, Mass. (1976).

4. S. J. Arnold, N. Finlayson, and E. A. Ogryzlo, "Some Novel Energy-Pooling Processes Involving $O_2(^1\Delta_g)$" J. Chem. Phys. 44, 2529 (1966).

5. R. G. Derwent, D. R. Kearns, and B. A. Thrush, "The Excitation of Iodine by Singlet Molecular Oxygen," Chem. Phys. Lett 6, 115 (1970).

6. R. G. Derwent and B. A. Thrush, "Measurements on $O_2(^1\Delta_g)$ and $O_2(^1\Sigma_g^+)$ in Discharge Flow Systems," Trans. Faraday Soc. 67, 2036 (1971).

7. R. G. Derwent and B. A. Thrush, "The Radiative Lifetime of the Metastable Iodine Atom $I(5^2P_{1/2})$," Chem. Phys. Lett. 9, 591 (1971).

8. R. G. Derwent and B. A. Thrush, "Excitation of Iodine by Singlet Molecular Oxygen," J. Chem. Soc., Faraday II 68, 720 (1972).

9. R. G. Derwent and B. A. Thrush, "Excitation of Iodine by Singlet Molecular Oxygen," Disc. Faraday Soc. 53, 162 (1972).

10. A. K. MacKnight and P. J. Modreski, Chemical Generation of Electronically Excited Oxygen, AFWL-TR-74-100, Air Force Weapons Laboratory, Kirtland AFB, New Mex. (1974); also, Laser Digest, Spring 1974.

11. R. D. Franklin, Kinetic Model of the Oxygen-Iodine Transfer Laser, AFWL-TR-74-241, Air Force Weapons Laboratory, Kirtland Air Force Base, New Mex. (1974); also, Laser Digest, Summer 1974.

12. D. G. Sutton and S. N. Suchard, "Potential Electronic Transition Chemical Laser: Parametric Evaluation," Appl. Opt. 14, 1898 (1975).

13. S. N. Suchard, The Aerospace Corporation, private communication (1976).

14. K. H. Becker, W. Groth, and U. Schurath, "The Quenching of Metastable $O_2(^1\Delta_g)$ and $O_2(^1\Sigma_g^+)$ Molecules," Chem. Phys. Lett. 8, 259 (1971).

15. L. J. Gillespie and L. H. D. Fraser, "The Normal Vapor Pressure of Crystalline Iodine," J. Amer. Chem. Soc. 58, 2260 (1936).

16. P. N. Clough and B. A. Thrush, Chem. Ind., 1971 (1966).

17. R. D. Hudson, A Critical Review of Ultraviolet Photoabsorption Cross Sections for Molecules of Astrophysical and Aeronomic Interest, NSRDS-NBS, National Bureau of Standards, Washington, D.C. (1971).

18. L. W. Bader and E. A. Ogryzlo, "Reactions of $O_2(^1\Delta_g)$ and $O_2(^1\Sigma_g^+)$," Disc. Faraday Soc. 37, 46 (1964).

19. L. Elias, E. A. Ogryzlo, and H. I. Schiff, "The Study of Electrically Discharged O_2 by Means of an Isothermal Calorimetric Detector," Canadian J. Chem. 37, 1680 (1959).

20. D. W. Trainor, D. O. Ham, and F. Kaufman, "Gas Phase Recombination of Hydrogen and Deuterium Atoms," J. Chem. Phys. 58, 4599 (1972).

21. R. F. Heidner III, and J. F. Bott, "Vibrational Deactivation of HF(v = 1) and DF(v = 1) by H and D Atoms," J. Chem. Phys. 63, 1810 (1975).

22. R. F. Heidner III, Quantitative Vacuum Ultraviolet Absorption Studies of Vibrationally Excited Hydrogen, Thesis, University of California, Los Angeles, 1972.

23. A. Fontijn, C. B. Meyer, and H. I. Schiff, "Absolute Quantum Yield Measurements of the NO-O Reaction and Its Use as a Standard for Chemiluminescent Reactions," J. Chem. Phys. 40, 64 (1964).

24. A. M. Falick and B. H. Mahan, "Collisional-Radiative Reaction of $O_2(^1\Delta_g)$," J. Chem. Phys. 47, 4778 (1967).

25. S. J. Arnold, E. A. Ogryzlo, and H. Witzke, "Some New Emission Bands of Molecular Oxygen," J. Chem. Phys. 40, 1769 (1964).

26. E. W. Gray and E. A. Ogryzlo, "The Cooperative Emission Bands of 'Singlet' Molecular Oxygen," Chem. Phys. Lett. 3, 658 (1969).

27. R. M. Badger, A. C. Wright, and R. F. Whitlock, "Absolute Intensities of the Discrete and Continuous Absorption Bands of Oxygen Gas at 1.26 and 1.065 μ and the Radiative Lifetime of the $^1\Delta_g$ State of Oxygen," J. Chem. Phys. 43, 4345 (1965).

28. J. H. Miller, R. W. Boese, and L. P. Giver, "Intensity Measurements and Rotational Distributions for the Oxygen A-Band," J. Quantitative Spectroscopy Radiative Transfer 9, 1507 (1969).

29. G. A. Capelle and H. P. Broida, "Lifetimes and Quenching Cross Sections of $I_2(B^3\Pi_{O_u^+})$," J. Chem. Phys. 58, 4212 (1973).

30. R. H. Garstang, "Transition Probabilities of Forbidden Lines," J. Res. NBS 68, 61 (1964).

31. E. Lissi and J. Heicklen, "The Photolysis of Ozone," J. Photochem. 1, 39 (1972/73).

32. R. J. Collins. D. Husain and R. J. Donovan, "Kinetic and Spectroscopic Studies of $O_2(a^1\Delta_g)$ by Time-Resolved Absorption Spectroscopy in the Vacuum Ultraviolet," J. Chem. Soc., Faraday II, 69, 145 (1973).

33. M. J. Kurylo, W. Braun, A. Kaldor, S. M. Freund, and R. P. Wayne, "*Infrared Laser Enhanced Reactions: Chemistry of Vibrationally-Excited* O_3 with NO and $O_2(^1\Delta)$," J. Photochem. 3, 71 (1974/75).

34. D. D. Davis, W. Wong, and J. Lephardt, "A Laser Flash-Photolysis-Resonance Fluorescence Kinetic Study: Reaction of $O(^3P)$ with O_3," Chem. Phys. Lett. 22, 273(1973).

35. M. Gauthier and D. R. Snelling, "Mechanism of Singlet Molecular Oxygen Formation from Photolysis of Ozone at 2537Å," J. Chem. Phys. 54, 4317 (1971).

36. D. J. Giachardi and R. P. Wayne, "The Photolysis of Ozone by Ultraviolet Radiation," Proc. Royal Soc., London A, 330, 131 (1972).

37. E. B. Turner, G. Emamuel, and R. L. Wilkins; TR-0059(6240-20)-1, THE NEST Chemistry Computer Program, Vol. I, The Aerospace Corporation, El Segundo, Calif. (1970).

38. L. R. Martin, R. B. Cohen; and J. F. Schatz, "Quenching of Laser-Induced Fluorescence of $O_2(^1\Sigma_g^+)$ by N_2 and O_2," Chem. Phys. Lett. 41, 394 (1976).

39. G. M. Lawrence, "Resonance Transition Probabilities in Intermediate Coupling for Some Neutral Non-Metals," Astrophys. J. 148, 261 (1967).

40. R. G. O. Thomas and B. A. Thrush, "Quenching of $O_2(^1\Sigma)$ by Ground State O_2," J. Chem. Soc., Faraday II 71, 664 (1975).

41. J. J. Deakin and D. Husain, "Temperature Dependence of Collisionally Induced Spin Orbit Relexation of $I(^2P_{1/2})$," J. Chem. Soc., Faraday II 68, 1603 (1972).

42. D. H. Burde, R. A. McFarlane, and J. R. Wiesenfeld, "Studies of the Deactivation of Electronically Excited Iodine Atoms," IEEE J, Quantum Electron. QE-11, 709 (1975).

43. R. J. Donovan and D. Husain, Reactions of Atoms and Small Molecules," Chemical Soc., London 68, 124 (1971).

APPENDIX A

CHEMICAL KINETICS OF THE $O_2(^1\Delta)$-I ATOM SYSTEM†

$$I + O_2(^1\Delta) \xrightarrow{k_1} I^* + O_2(^3\Sigma) \qquad \text{(A-1)}$$

$$I^* + O_2(^1\Delta) \xrightarrow{k_2} I + O_2(^1\Sigma) \qquad \text{(A-2)}$$

$$I^* \xrightarrow{k_3} I + h\nu \qquad \text{(A-3)}$$

$$O_2(^1\Sigma) \xrightarrow{k_4} O_2(^3\Sigma) + h\nu \qquad \text{(A-4)}$$

$$I^* + O_2(^3\Sigma) \xrightarrow{k_5} I + O_2(^1\Delta) \qquad \text{(A-5)}$$

$$I^* + O_2(^3\Sigma) \xrightarrow{k_6} I + O_2(^3\Sigma) \qquad \text{(A-6)}$$

$$I + O_2(^1\Delta) \xrightarrow{k_7} I + O_2(^3\Sigma) \qquad \text{(A-7)}$$

$$I^* + M \xrightarrow{k_8} I + M \qquad \text{(A-8)}$$

$$O_2(^1\Delta) + O_2(^1\Delta) \xrightarrow{k_9} O_2(^1\Sigma) + O_2(^3\Sigma) \qquad \text{(A-9)}$$

$$O_2(^1\Sigma) + \text{wall} \xrightarrow{k_{10}} O_2(^1\Delta) + \text{wall} \qquad \text{(A-10)}$$

$$I^* + \text{wall} \xrightarrow{k_{11}} I + \text{wall} \qquad \text{(A-11)}$$

$$O_2(^1\Delta) + \text{wall} \xrightarrow{k_{12}} O_2(^3\Sigma) + \text{wall} \qquad \text{(A-12)}$$

$$O_2(^1\Delta) + M \xrightarrow{k_{13}} O_2(^3\Sigma) + M \qquad \text{(A-13)}$$

$$O_2(^1\Sigma) + M \xrightarrow{k_{14}} O_2(^1\Delta) + M \qquad \text{(A-14)}$$

† In so far as possible, the above reactions are numbered as they appear in Ref. 9.

$$I_2(^1\Sigma) + O_2(^1\Sigma) \xrightarrow{k_{15}} O(^3\Sigma) + 2I \qquad \text{(A-15)}$$

$$I_2(^1\Sigma) + O_2(^1\Sigma) \xrightarrow{k_{16}} O_2(^3\Sigma) + I_2(^3\Pi_{1u}) \qquad \text{(A-16)}$$

$$I_2(^3\Pi_{1u}) + O_2(^1\Delta) \xrightarrow{k_{17}} I_2(^3\Pi_{O_u^+}) + O_2(^3\Sigma) \qquad \text{(A-17)}$$

$$I \text{ or } I^* + \text{wall} \xrightarrow{k_{18}} 1/2\ I_2 + \text{wall} \qquad \text{(A-18)}$$

APPENDIX B

ANALYTIC SOLUTIONS TO THE $O_2(^1\Delta)$-I ATOM KINETIC EQUATIONS

A. STEADY-STATE CONCENTRATION OF I^*

$$\frac{-d[I^*]}{dt} = k_3[I^*] + k_2[I^*][O_2(^1\Delta)] + (k_5 + k_6)[I^*][O_2(^1\Delta)] + k_{11}[I^*] - k_1[I][O_2(^1\Delta)] \tag{B-1}$$

with $d[I^*]/dt = 0$,

$$[I^*] = \frac{k_1[I][O_2(^1\Delta)]}{k_3 + k_2[O_2(^1\Delta)] + (k_5 + k_6)[O_2(^3\Sigma)] + k_{11}} \tag{B-2}$$

With the rate coefficients given in Appendix C, it can be shown that $(k_5 + k_6)[O_2(^3\Sigma)]$ outweighs all other possible terms in the denominator. Thus,

$$\frac{[I^*]}{[I]} = \frac{k_1}{(k_5 + k_6)} \frac{[O_2(^1\Delta)]}{[O_2(^3\Sigma)]} \tag{B-3}$$

The rate coefficients k_1 and k_5 are related by an equilibrium constant defined by statistical mechanics. If $k_6 \ll k_5$, a very simple expression results, i.e.,

$$\frac{[I^*]}{[I]} = K_{EQ} \frac{[O_2(^1\Delta)]}{[O_2(^3\Sigma)]} \tag{B-4}$$

The term $K_{EQ} = 2.88$ at T = 295 K (see text).

B. TIME DEPENDENCE OF $O_2(^1\Delta)$

$$\frac{-d[O_2(^1\Delta)]}{dt} = (k_1 + k_7)[I][O_2(^1\Delta)] + k_2[I^*][O_2(^1\Delta)] + k_9[O_2(^1\Delta)]^2$$

$$- k_5[I^*][O_2(^3\Sigma)] - k_{10}[O_2(^1\Sigma)] \qquad \text{(B-5)}$$

Derwent and Thrush[8] found that $-d[O_2(^1\Delta)]/dt$ is first order in both $[I]$ and $[O_2(^1\Delta)]$. This eliminates the second, third, and last terms, all of which depend upon $[O_2(^1\Delta)]^2$. With those terms dropped and Eq. (B-3) substituted into (B-5)

$$\frac{-d[O_2(^1\Delta)]}{dt} = \frac{[(k_1 + k_7) - k_1k_5]}{(k_5 + k_6)}[I][O_2(^1\Delta)] = \left\{\frac{k_1k_6}{(k_5 + k_6)} + k_7\right\}[I][O_2(^1\Delta)]$$

(B-6)

Thus, a plot of $\ln[O_2(^1\Delta)]$ versus t at constant $[I]$ yields a value for $k_1k_6/(k_5 + k_6) + k_7$. Derwent and Thrush found this quantity to be $(8 \pm 1) \times 10^{10}$ cm^3/mol-sec. Using independently determined values for k_5 and k_1, they were able to demonstrate the following inequalities:

$$k_6 = 4.4 \times 10^9 k_3 - \frac{k_3k_7}{18} \leq 3.4 \times 10^{10} \text{ cm}^3/\text{mol-sec}$$

$$k_7 \leq 8 \times 10^{10} \text{ cm}^3/\text{mol-sec} \qquad \text{(B-7)}$$

The branching ratio for I^* removal by electronic energy transfer (k_5) versus quenching (k_6) is

$$\frac{k_5}{k_6} \geq 470 \qquad \text{(B-8)}$$

C. STEADY-STATE DENSITY OF $O_2(^1\Sigma)$

In the absence of added I_2, $O_2(^1\Sigma)$ is formed by Process (A-9) [$O_2(^1\Delta)$ energy pooling] and is deactivated at the flow tube walls (A-10). Under certain conditions, gas phase quenching (A-14) may become comparable to wall deactivation, but it will be ignored in this analysis.

The $[O_2(^1\Sigma)]$ can be solved for in the absence of I_2.

$$[^1\Sigma]^0 = \frac{[^1\Delta]^2 k_9}{k_{10}} \tag{B-9}$$

When I_2 is present

$$\frac{d[^1\Sigma]}{dt} = k_9[^1\Delta]^2 + k_2[I^*][^1\Delta] - (k_{15} + k_{16})[^1\Sigma][I_2] - k_{10}[^1\Sigma] = 0 \tag{B-10}$$

$$[^1\Sigma] = \frac{(^1\Delta)^2\left(k_9 + \left\{k_2[I^*]/[^1\Delta]\right\}\right)}{k_{10} + (k_{15} + k_{16})[I_2]} \tag{B-11}$$

$$\frac{[^1\Sigma]}{[^1\Sigma]^0} = \frac{\left(\left[1 + k_2k_1/k_9(k_5 + k_6)\right]\left\{[I]/[O_2(^3\Sigma)]\right\}\right)}{1 + \left\{(k_{15} + k_{16})[I_2]\right\}/k_{10}} \tag{B-12}$$

Under special circumstances discussed by Derwent and Thrush and in Section V.B.3 of this report, the above expression may be approximated as

$$\frac{[^1\Sigma]}{[^1\Sigma]^0} - 1 = \frac{k_2k_1}{k_9(k_5 + k_6)} \frac{[I]}{[O_2(^3\Sigma)]} \tag{B-13}$$

D. STEADY-STATE DENSITY OF I_2

$$\frac{-d[I_2]}{dt} = (k_{15} + k_{16})[I_2][O_2(^1\Sigma)] - \frac{k_{18}}{2}\left([I] + [I^*]\right) = 0 \qquad \text{(B-14)}$$

Since $[I_2]^0 - [I_2] = 1/2([I^*] + [I])$, by suitable arrangement,

$$\frac{[I_2]}{[I_2]^0} = \frac{1}{1 + [(k_{15} + k_{16})/k_{18}][O_2(^1\Sigma)]} \qquad \text{(B-15)}$$

is obtained.

APPENDIX C

RATE COEFFICIENTS FOR THE KINETIC MODEL OF APPENDIX A

Process	k	Ref.
k_1	$(4.6 \pm 1.5) \times 10^{13} cm^3/mol\text{-}sec$	9
k_2	$(1.6 \pm 0.2) \times 10^{10} cm^3/mol\text{-}sec$	9
k_3	$7.8\ sec^{-1}$	30
k_4	$0.077\ sec^{-1}$	28
k_5	$(1.6 \pm 0.5) \times 10^{13} cm^3/mol\text{-}sec$	9
k_6	$3.4 \times 10^{10} cm^3/mol\text{-}sec$	8
k_7	$8 \times 10^{10} cm^3/mol\text{-}sec$	8
k_8		See Appendix D
k_9	$1.2 \times 10^{7} cm^3/mol\text{-}sec$	6
k_{10}	$\gamma_{10} \approx 1 \times 10^{-2}$	6
k_{11}	$\gamma_{11} \approx 1$	-
k_{12}	$\gamma_{12} \approx 2 \times 10^{-5}$	6
k_{13}		See Appendix D,
k_{14}		See Appendix D
k_{15}	$1 \times 10^{14} cm^3/mol\text{-}sec$	8
k_{16}	$4 \times 10^{13} cm^3/mol\text{-}sec$	8
k_{17}		
k_{18}	$\gamma_{18}(\text{pyrex}) \approx 1$;	
	$\gamma_{18}(\text{Halocarbon}) \approx 10^{-3}$	This work

APPENDIX D

RATE COEFFICIENTS FOR QUENCHING OF $O_2(^1\Delta)$, $O_2(^1\Sigma)$, AND I^*

Quencher	$O_2(^1\Delta)$, k(cm^3/mol-sec)	Ref.	$O_2(^1\Sigma)$, k(cm^3/mol-sec)	Ref.	I^*, k(cm^3/mol-sec)	Ref.
Ar	6×10^3	14	9×10^6	14	$< 1.2 \times 10^6$	43
	5.4×10^3	32				
He	6×10^3	14	6×10^6	14	$< 3 \times 10^6$	43
	4.8×10^3	32				
SF_6	6×10^3	14	9×10^8	14	1.9×10^9	43
					1.4×10^7	43
N_2	6×10^3	14	1.3×10^9	14	1.3×10^7	43
	8.4×10^4	32		38	3.9×10^6	43
O_2	1.0×10^6	14	9×10^7	14	1.6×10^{13}	43
H_2O	2.4×10^6	14	3.0×10^{12}		5.7×10^{11}	43
O_3	2.2×10^9	33	4.2×10^{12}	14	--	--
	2.6×10^9	32				
I_2	--	--	2×10^{14}	8	2.5×10^{12}	41
					2.2×10^{13}	42

APPENDIX E

SAMPLE CALCULATION FOR PRODUCTION OF POPULATION INVERSION IN I ATOM

A. DISCHARGED O_2 CALIBRATION

1. Dimol sensitivity constant = 1.8×10^6 Hz-Torr^{-2}
2. Experimental conditions: P_{O_2} = 2.472 Torr; $\dot{m}_{O_2}$ = 4.75 L-Torr/sec; $I_{6340} = 5 \times 10^4$ Hz; $P_{^1\Delta}$ = 0.167 Torr; $P_{^3\Sigma}$ = 2.305 Torr.
3. $O_2(^1\Delta)/O_2(^3\Sigma) = 0.0725$; thus, I^*/I (predicted) = 2.9(0.0725) = 0.21.
4. Calibration of Ge detector for $O_2(^1\Delta)$ at 1.27 μm = 55 mTorr/mV.

B. I_2 ADDITION TO DISCHARGED O_2

1. $\dot{m}_{He + I_2}$ = 0.122 L-Torr/sec
2. $P_{He + I_2}$ = 0.0625 Torr
3. Mole fraction of I_2 in He at T = 298 K = 3.1×10^{-4}
4. $P_{I_2} = 1/2\,(P_I + I^*) = 1.95 \times 10^{-5}$ Torr
5. $I_{1.27}/I_{1.315} = 0.836$ with Eq. (21) used; $I^*/^1\Delta = 3.36 \times 10^{-5}$
6. $P_I^* = 5.5 \times 10^{-6}$ Torr; $P_I = 3.35 \times 10^{-5}$ Torr
7. I^*/I (measured) ≈ 0.17

C. I_2 ADDITION TO PHOTOLYZED O_3

1. Experimental conditions: photolysis temperature = -28°C; $\dot{m}_{N_2}$ = 1.375 L-Torr/sec; $\dot{m}_{He + I_2}$ = 0.122 L-Torr/sec; P_{total} = 2.000 Torr; $P_{He + I_2}$ = 0.163 Torr; $P_{I + I^*} = 1.02 \times 10^{-4}$ Torr; P_{N_2} = 1.804 Torr; P_{O_2} (≡ 3/2 P_{O_3}) = 0.033 Torr.

2. $I_{6340} = 125$ Hz → 8.3 mTorr $O_2(^1\Delta)$

$I_{1.27_1} = 120\ \mu V$ → 6.6 mTorr $O_2(^1\Delta)$

3. $P_{O_2}(^1\Delta) \approx 7.5$ mTorr

$P_{O_2}(^3\Sigma) \approx 25.5$ mTorr

$O_2(^1\Delta)/O_2(^3\Sigma) = 0.29$

I^*/I (predicted) = (2.9)(0.29) = 0.86

$I_{1.27}/I_{1.315} = 4.7 \times 10^{-3}$

Using Eq. (21), $I^*/O_2(^1\Delta) = 6.0 \times 10^{-3}$

$P_I^* = 4.5 \times 10^{-5}$ Torr

$P_I = 5.7 \times 10^{-5}$ Torr

I^*/I (measured) = 0.79

THE IVAN A. GETTING LABORATORIES

The Laboratory Operations of The Aerospace Corporation is conducting experimental and theoretical investigations necessary for the evaluation and application of scientific advances to new military concepts and systems. Versatility and flexibility have been developed to a high degree by the laboratory personnel in dealing with the many problems encountered in the nation's rapidly developing space and missile systems. Expertise in the latest scientific developments is vital to the accomplishment of tasks related to these problems. The laboratories that contribute to this research are:

Aerophysics Laboratory: Launch and reentry aerodynamics, heat transfer, reentry physics, chemical kinetics, structural mechanics, flight dynamics, atmospheric pollution, and high-power gas lasers.

Chemistry and Physics Laboratory: Atmospheric reactions and atmospheric optics, chemical reactions in polluted atmospheres, chemical reactions of excited species in rocket plumes, chemical thermodynamics, plasma and laser-induced reactions, laser chemistry, propulsion chemistry, space vacuum and radiation effects on materials, lubrication and surface phenomena, photosensitive materials and sensors, high precision laser ranging, and the application of physics and chemistry to problems of law enforcement and biomedicine.

Electronics Research Laboratory: Electromagnetic theory, devices, and propagation phenomena, including plasma electromagnetics; quantum electronics, lasers, and electro-optics; communication sciences, applied electronics, semiconducting, superconducting, and crystal device physics, optical and acoustical imaging; atmospheric pollution; millimeter wave and far-infrared technology.

Materials Sciences Laboratory: Development of new materials; metal matrix composites and new forms of carbon; test and evaluation of graphite and ceramics in reentry; spacecraft materials and electronic components in nuclear weapons environment; application of fracture mechanics to stress corrosion and fatigue-induced fractures in structural metals.

Space Sciences Laboratory: Atmospheric and ionospheric physics, radiation from the atmosphere, density and composition of the atmosphere, aurorae and airglow; magnetospheric physics, cosmic rays, generation and propagation of plasma waves in the magnetosphere; solar physics, studies of solar magnetic fields; space astronomy, x-ray astronomy; the effects of nuclear explosions, magnetic storms, and solar activity on the earth's atmosphere, ionosphere, and magnetosphere; the effects of optical, electromagnetic, and particulate radiations in space on space systems.

THE AEROSPACE CORPORATION
El Segundo, California